INTERNATIONAL CENTRE FOR THEORETICAL PHYSICS
I.C.T.P., P.O. BOX 586, 34100 TRIESTE, ITALY, CABLE: CENTRATOM TRIESTE

H4.SMR/775-8

COLLEGE IN BIOPHYSICS: EXPERIMENTAL AND THEORETICAL ASPECTS OF BIOMOLECULES

26 September - 14 October 1994

Miramare - Trieste, Italy

Electron Transfer Reaction

J.N. Onuchic
University of California at San Diego
La Jolla, CA, USA

ELECTRON TRANSFER REACTIO

J. N. ONUCHIC

I-

UNIMOLECULAR REACTIONS

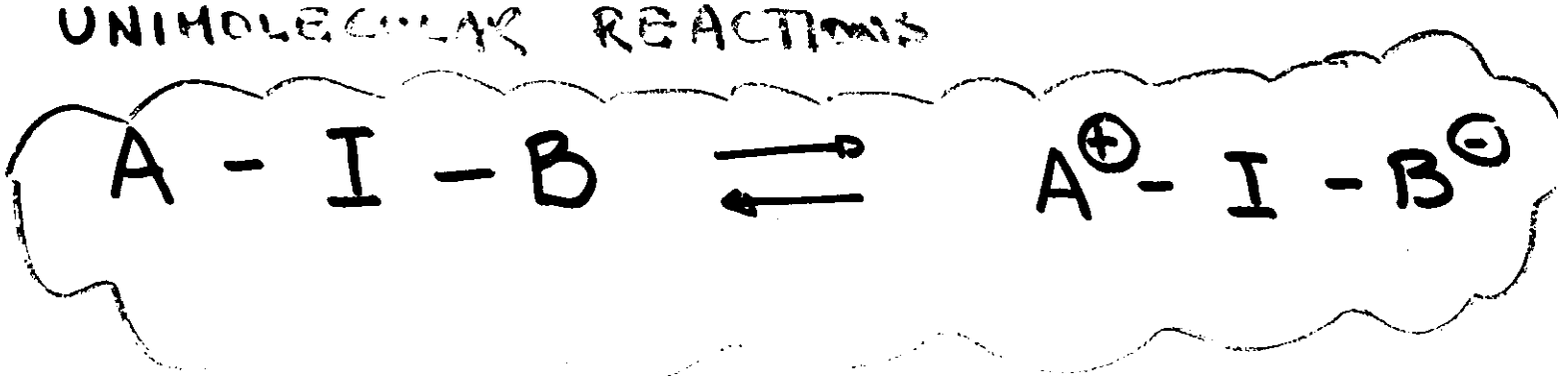

What molecular details of A and B and of the surrounding medium determine the transfer rate and tunneling pathways between spaces.

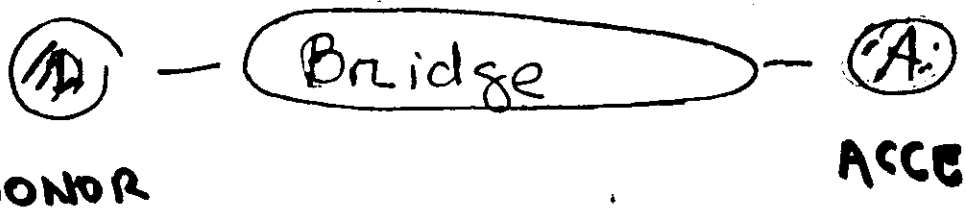

DONOR	BRIDGE	ACCEPTOR
Chlorophyll$_2^*$	Protein	Ubiquinone
Impurity	Semiconductor	Impurity
$Ru^{+2}(bipy)_3^*$	Solvent	$Ru^{+2}(NH_3)_5$
Electrode	Surface	Ion
Porphyrin	Linker	Quinone
e^-_{aq}	Glass	Organic Molecule

- More specifically we are interested in :
- The influence of the "stuff" inbetween on k_{ET}.
- The ΔG dependence of the rate.
- Separability of the above two.

A. $Fe^{2+}(H_2O)_6 + Fe^{3+}(H_2O)_6 \longrightarrow Fe^{3+}(H_2O) + Fe^{2+}(H_2$

B. $K + Br_2 \longrightarrow K^+ + Br_2^-$ (gas pha

C. 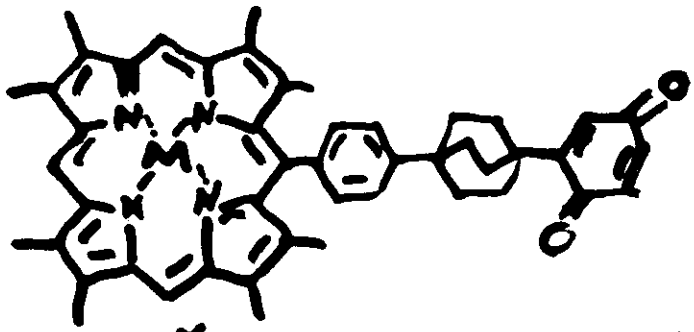

$\rightleftharpoons P^+ Q^-$

P^* Q

D. 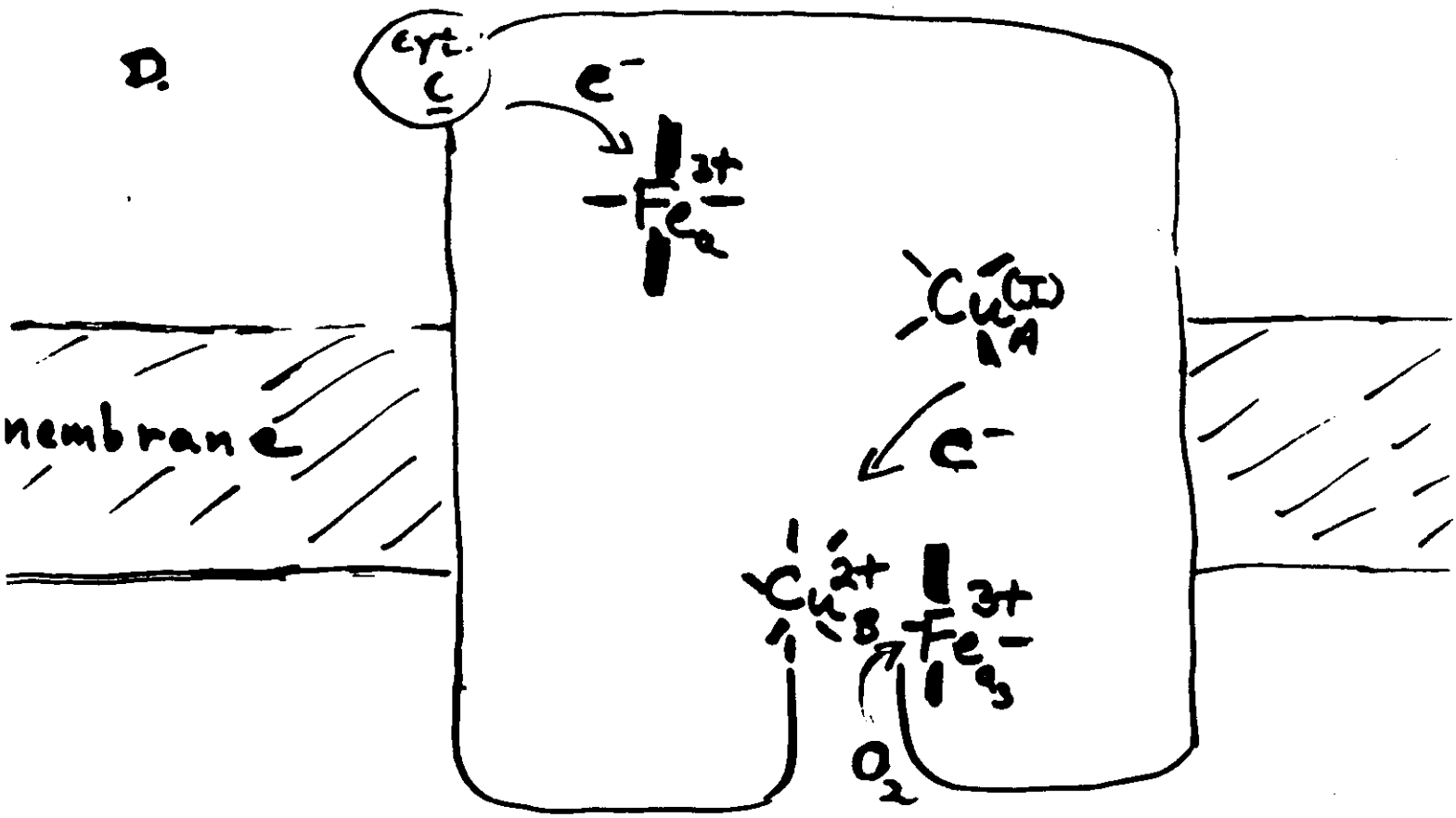

E. Photosynthetic Reaction Center

It will be discussed in details during the coorse

cyt c $BChl_2$ BPh Q

Energetics of the Primary Electron transfer Process

Rhodopseudomonas Spaheroides

- DISCUSS ALL RATES IN THE BOARD
- QUANTUM EFFECTS

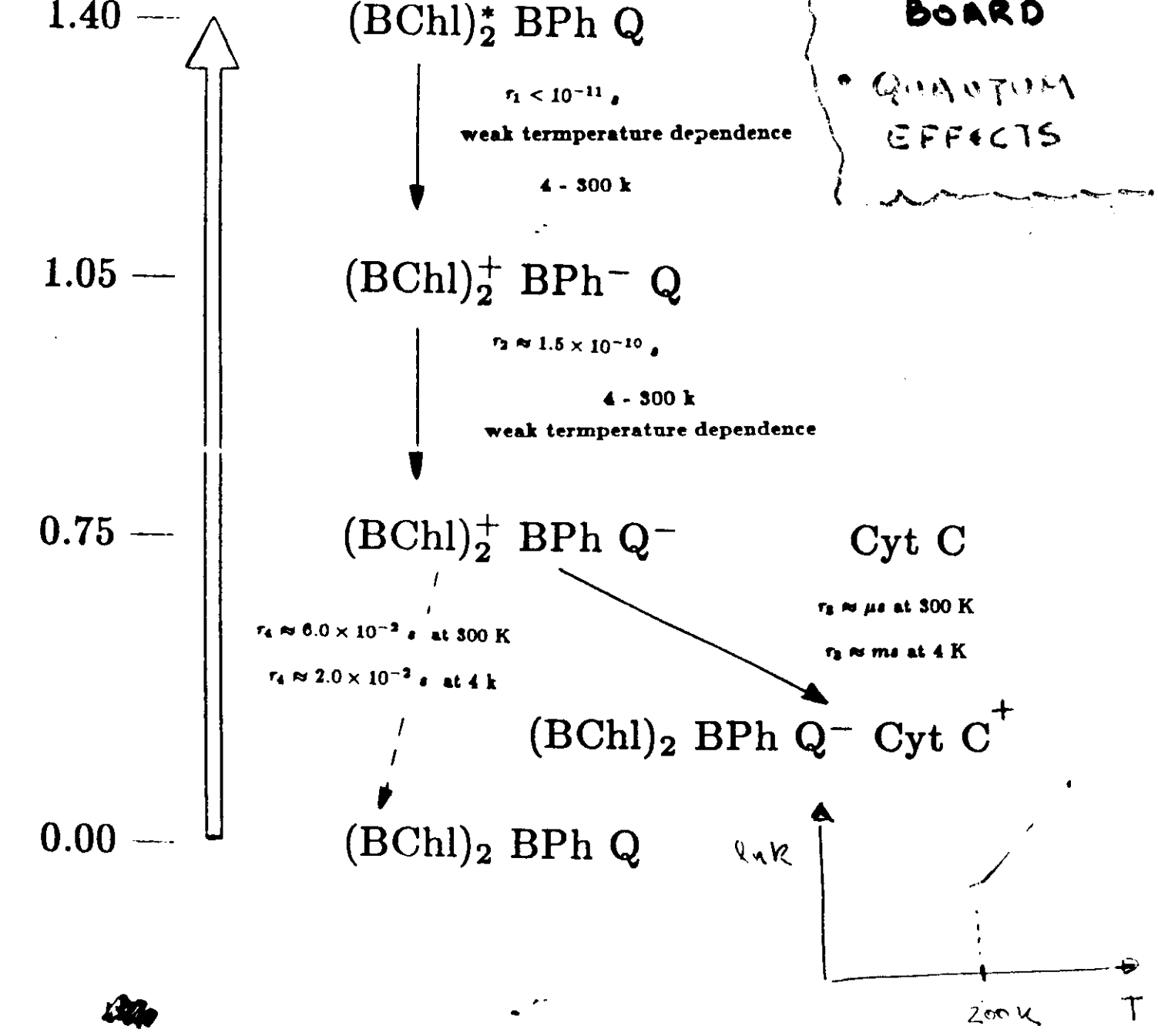

III - WHY STUDY E.T. REACTIONS ?

- SIMPLEST CHEMICAL REACTION
- NO BONDS MADE OR BROKEN.
  UNIMOLECULAR
  UBIQUITOUS IN CHEMISTRY AND BIOLOGY
- QUANTUM CONTROL OF BIOLOGICAL PROCESSES
- If we can't understand these we might as well throw in the towel

---

IV - FORMULATION OF THE PROBLEM

1. DEFINE DONOR-ACCEPTOR CONFIGURATION
2. DEFINE the Initial and final states
3. Solve (in principle, anyway) $H\Psi = E\Psi$ for the initial and final electronic states within the Born-Oppenheimer Approx.
4. !!! Evolution from initial to final states !!!

V - EXAMPLE

A. Digression on Potential Energy Surfaces.

Solving a molecular eigenvalue problem in the Born-Oppenheimer approximation gives an <u>electronic</u> energy dependent on the nuclear coordinate (Reaction Coordinate), Q: $E^{el}(Q)$

So we obtain a potential Energy surface by:

$$U(Q) = E^{el}(Q) + V^{nucl.}(Q) = \text{POTENTIAL NUCLEI FEEL}$$

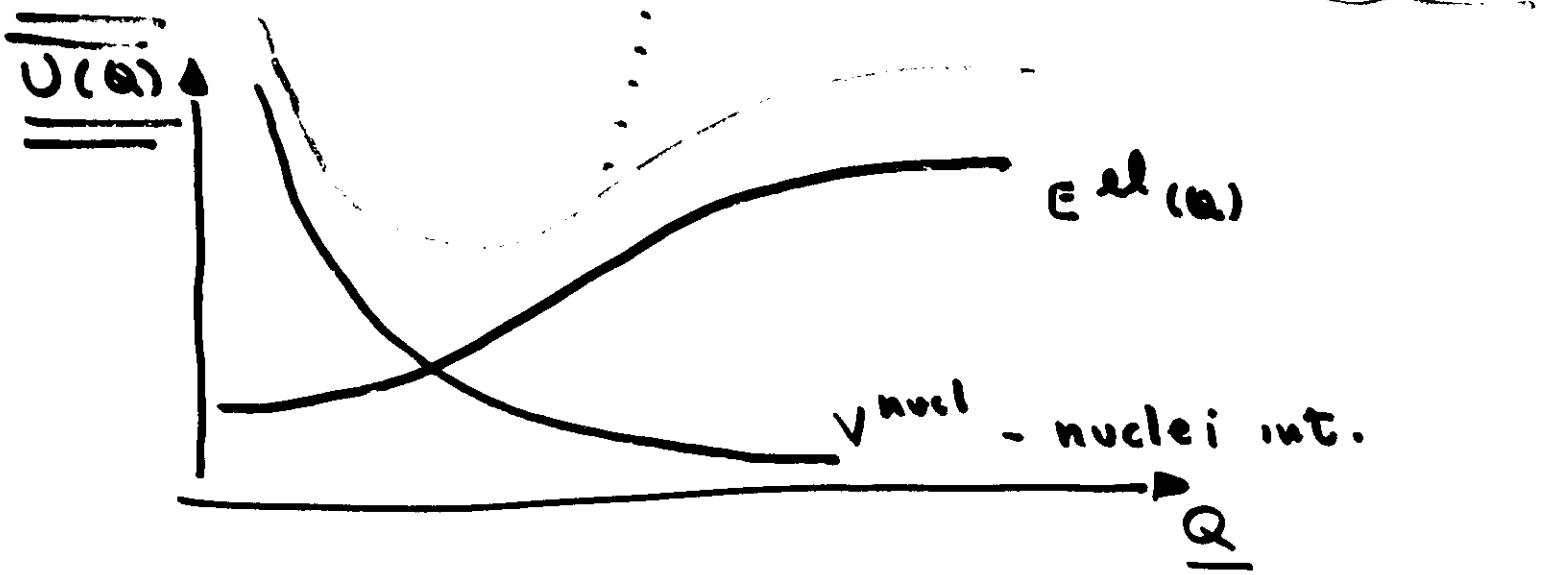

CONDON

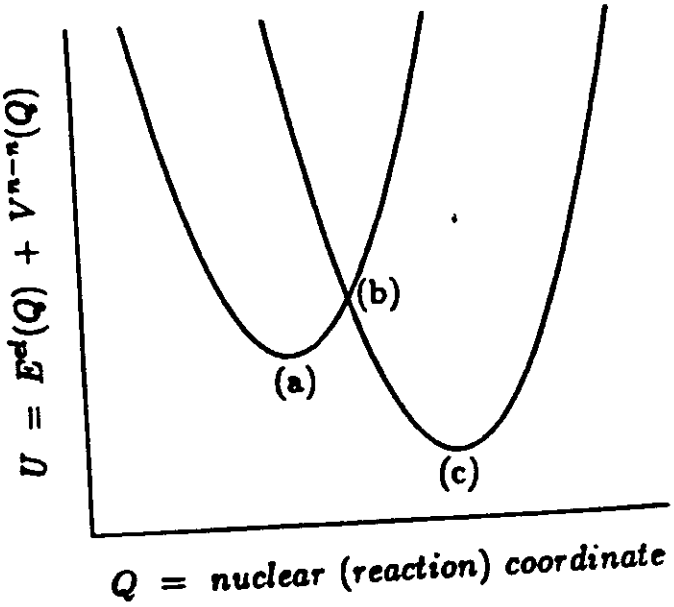

non-adiabatic surfaces

$H' = 0$
correct zero order picture (no couplin

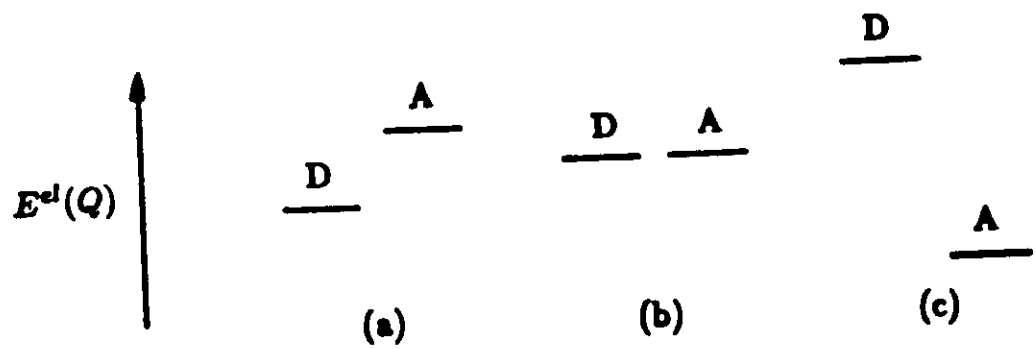

(b)

- Since system insensitive to Q_A

  Forget it, just worry about the electronic energy difference between reactant and products (R and P) in the donor site

- Also there is no wall between donor and acceptor so there is an exchange parameter V mixing initial and final states

- V - tunneling matrix element - TOPIC OF NEXT WEEK

Thus: $U_{nuc} = U(Q_A) + U(Q_B)$

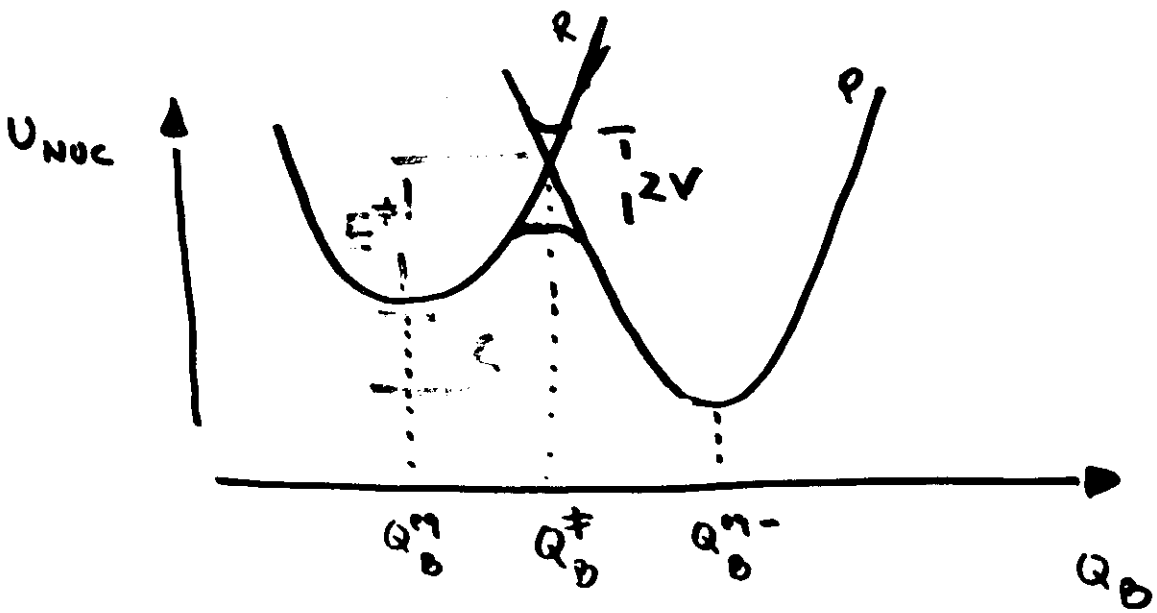

ε - driving force or energy gap

E^* - ACTIVATION ENERGY

$$U^R(Q_b) = \varepsilon_1 + \frac{1}{2} M \Omega^2 \left(Q_b - Q_b^{eq} \right)^2$$

$$U^P(Q_b) = \varepsilon_2 + \frac{1}{2} M \Omega^2 \left(Q_b - Q_b^{eq-} \right)^2$$

- $\varepsilon = \varepsilon_1 - \varepsilon_2 =$ driving Force

---

- $\lambda = \frac{1}{2} M \Omega^2 \left(Q_b^{eq} - Q_b^{eq-} \right)^2 \rightarrow$ Reorganization energy

---

- $F = \frac{dU^R}{dQ_b} - \frac{dU^P}{dQ_b} = M \Omega^2 \left(Q_b^{eq-} - Q_b^{eq} \right)$

CONDON APPROXIMATION

$$V(Q_b) \sim V(Q_b^{\ddagger})$$

since transfer only occurs at $Q_b^{\ddagger}$

V Large

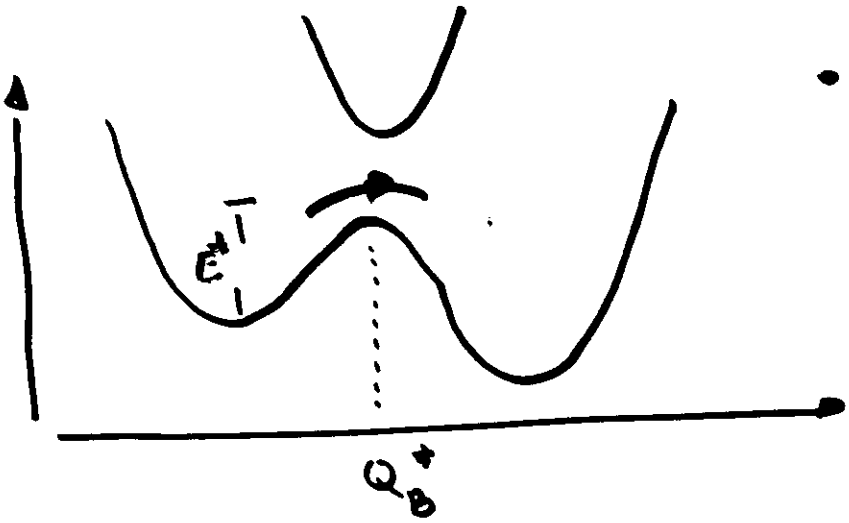

• CONVENTIONAL CHEMISTRY

Reaction adiabatic

every crossing through $Q_B^{\neq}$ goes R ⟷ P

V small

Reaction non-adiabatic

GOING FROM R TO P has a small probability proportional to V^2 when crossing Q_B^+

Questions !

- What is V small or large !

  non-adibaticity vs. adiabaticity

- How the systems decides if it is in R or P?

  quantum friction

Theory of E.T.

The Born - Oppenheimer approximation

J.N. ONUCHIC
Physics 206

Full Hamiltonian

$$H = \frac{P_R^2}{2M} + \frac{P_e^2}{2m} + V(r_e, R) + V_N(R)$$

Find eigenstates

$$H \Psi_{ij}(r_e, R) = E_{ij} \Psi_{ij}(r_e, R) \quad (1)$$

i and j are the quantum #s.

eigenstates of H are $\Psi_{ij}(r_e, R) = \varphi_i(r_e; R)\, \phi_{ij}(R)$ (2)

To compute φ_i we consider only the electronic part of the hamiltonian and R as a parameter

$$H_{el} = \frac{P_e^2}{2m} \quad V(r_e, R)$$

eigenstates of H_{el} are

$$H_{el} \varphi_i(r_e; R) = \mathcal{E}_{el}^i(R)\, \varphi_i(r_e; R) \quad (3)$$

Substituting (2) → (1), and using (3) we get

$$H \Psi_{ij}(r_e, R) = \frac{P_R^2}{2M} \cdot \varphi_i(r_e; R) \cdot \phi_{ij}(R) + H_{el}\, \varphi_i \phi_{ij} + V_N(R)\, \varphi_i \phi_{ij}$$

$$= E\, \varphi_i \phi_{ij}$$

Making the approximation

$$\frac{P_R^2}{2M}\,\varphi_i\,\phi_{ij} \approx \varphi_i\,\frac{P_R^2}{2M}\,\phi_{ij}$$

Assuming that φ_i varies slowly in R → This is the B.O approximation and people should read about its validity. It works when nuclei move much slower than the electron.

If this is appropriate, then ϕ_{ij} can be obtained from

$$\frac{P_R^2}{2M}\,\phi_{ij}(R) + \left[\mathcal{E}_{el}^{i}(R) + V_N(R)\right]\phi_{ij}(R) = E\,\phi_{ij}(R)$$

effective potential seen by the nuclei

Toy Model For electron transfer

x - electronic coordinate

y - nuclear coordinate

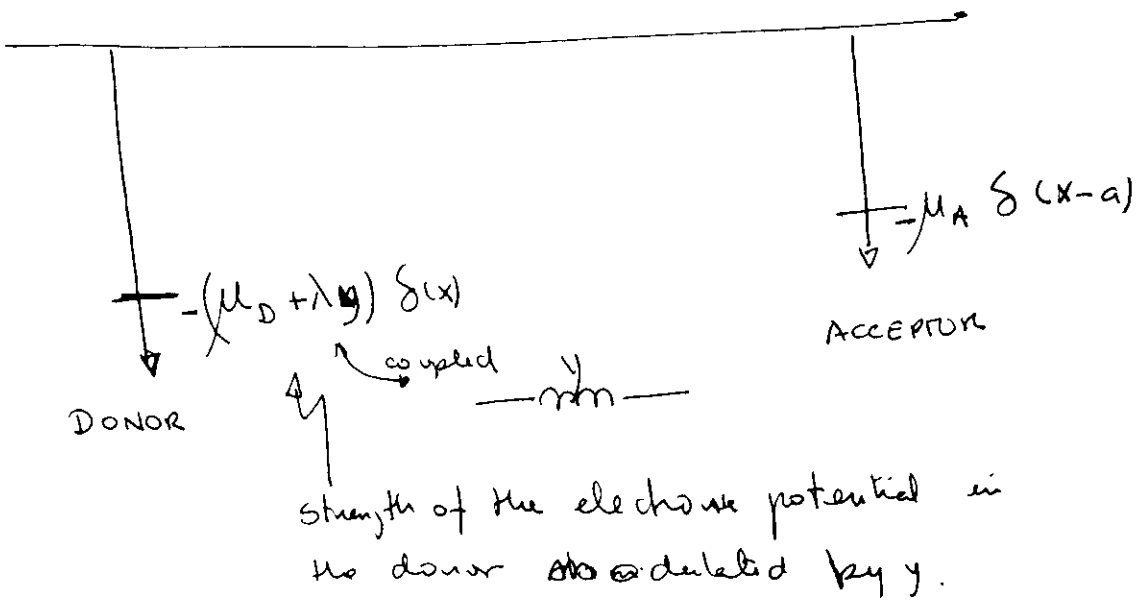

Full Hamiltonian

$$H = \frac{P_x^2}{2m} + (\mu_D + \lambda y)\delta(x) - \mu_A \delta(x-a) + \frac{P_y^2}{2M} + \frac{1}{2} M \Omega^2 y^2$$

Now we solve the problem in two approximation

1 - e^- in donor — neglect acceptor site

2 - e^- in acceptor - neglect donor site

Case (1) (4)

$$H_{DONOR} = \frac{P_x^2}{2m} - (\mu_D + \lambda y)\,\delta(x) + \frac{P_y^2}{2M} + \frac{1}{2} M \Omega^2 y^2$$

$$\Psi_{DONOR} = \Psi_{el}^{a}(x;y)\,\phi(y)$$

Solving for the electron part

$$\left[\frac{P_x^2}{2m} - (\mu_D + \lambda y)\,\delta(x)\right] \Psi_{el} = \epsilon_{el}(y)\,\Psi_{el}$$

Solution for a delta function with y as a parameter

$$\epsilon_{el}(y) = -\frac{m}{2\hbar^2}(\mu_D + \lambda y)^2 \qquad \Psi_{el}(x;y) = e^{-\frac{m}{\hbar^2}(\mu_D + \lambda y)|x|}$$

To make a simple approximation we neglect the quadratic term in y (if the quadratic term is kept it would give a small correction to the curvature of the parabola for $V_D(y)$)

$$\epsilon_{el}(y) \approx -\frac{m}{2\hbar^2}\mu_D^2 - \underbrace{\frac{m}{\hbar^2}\mu_D \lambda}_{g}\, y$$

Thus the nuclear potential for the nuclei when $\bar{e}$ is in the donor

$$V_D(y) = \epsilon_{el}(y) + V_N(y) = \frac{1}{2} M \Omega^2 y^2 - g y - \frac{m \mu_D^2}{2\hbar^2} \qquad (4)$$

Case (2)

e^- in acceptor

$$V_A(y) = \frac{1}{2} m\Omega^2 y^2 - \frac{m\mu_A^2}{2\hbar^2} \qquad (5)$$

eqs (4) and (5) give the "Marcus" potential wells

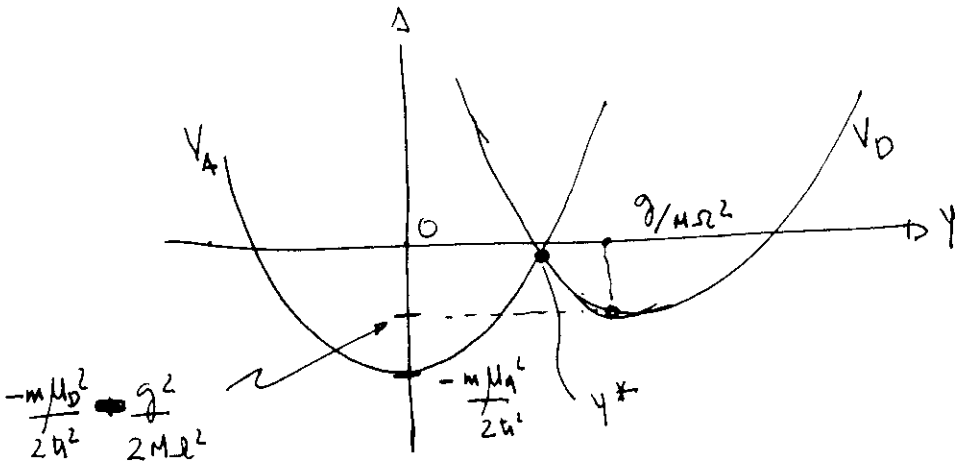

ON THE LEVEL OF APPROXIMATION we are using

Two surfaces ~~match~~ cross when $\boxed{y^* = \frac{(\mu_A - \mu_D)}{\lambda}}$

That's exactly the point that the point where the energy levels match on the figure on page 3 for the two delta wells.

electron transfer will happen only when the levels match → resonance.

Thus, 2 approximations have been made

1 - Born oppenheimer

2 - Condon — electronic transitions occur only with fixed nuclear coordinates.

γ^* is the only point that energy is conserved for the same γ for donor and acceptor

The question now is how we compute the electronic coupling between these two electronic states at this point.

!! Before we do that please solve problems from my list !!!

References for this lecture:

* J. Jortner, Biochim. Biophys. Acta 594, 193, 1980

J. J. Hopfield, Proc. Nat Acad. Sci U.S.A 71, 3640, 1974

D. Devault, "Quantum Mechanical Tunneling in Biology", Cambridge Univ. Press, N.Y., 1984

R.A. Marcus and N. Sutton, Biochim Biophys Acta 811, 265, 198

Problem Set

(1) For the following problem

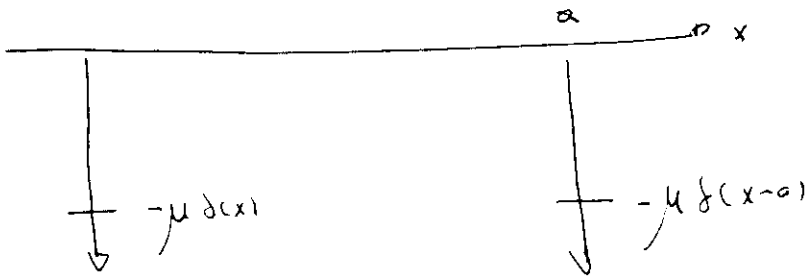

a) Compute the eigenstates of the problem

b) Create a wave packet localized around $x=0$ and calculate its time evolution.

(2) For the following tight binding H: (two level system)

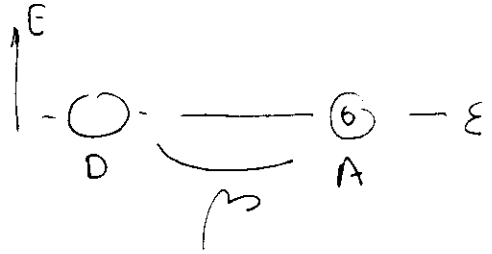

$$H = \varepsilon a_D^\dagger a_D + \varepsilon a_A^\dagger a_A + \beta\,(a_D^\dagger a_A + a_A^\dagger a_D)$$

if $\Psi_i = a_D^\dagger |0\rangle$

compute the time evolution, $P_D(t)$, $P_A(t)$

(3) For the 3 level system

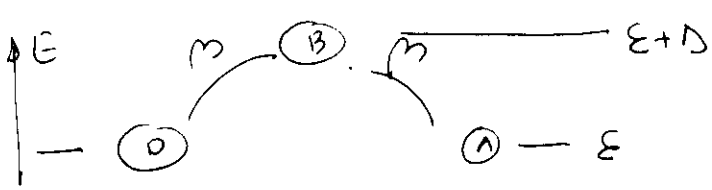

$$H: \varepsilon a_D^\dagger a_D + \varepsilon a_A^\dagger a_A + (\varepsilon+\Delta)\, a_B^\dagger a_B + \beta(a_D^\dagger a_B + a_B^\dagger a_D) + \beta(a_A^\dagger a_B + a_B^\dagger a_A)$$

if $\Psi_i = a_D^\dagger |0\rangle$

compute the time evolution, $P_D(t)$, $P_A(t)$

SPECIAL PROBLEM

(4) For H_{DONOR}, given in the top of pg 4, find the full. B.O. and exact solution for Ψ_{DONOR}.

PATHWAY ANALYSIS OF PROTEIN ELECTRON-TRANSFER REACTIONS

José Nelson Onuchic[1]

Department of Physics, University of California, San Diego, La Jolla, California 92093

David N. Beratan[2]

Jet Propulsion Laboratory, California Institute of Technology, Pasadena, California 91109, and Beckman Institute, California Institute of Technology, Pasadena, California 91125

Jay R. Winkler and Harry B. Gray

Beckman Institute, California Institute of Technology, Pasadena, California 91125

KEY WORDS: electron-tunneling pathways, electron coupling, ruthenium-modified proteins, cytochrome *c*, myoglobin

CONTENTS

[1] This review was begun when JNO was in residence at the Instituto de Fisica e Quimica de São Carlos, Universidade de São Paulo, 13560 São Carlos, S.P., Brazil.

[2] Present address: Department of Chemistry, University of Pittsburgh, Pittsburgh, Pennsylvania 15260.

1056-8700/92/0610-0349$02.00

PERSPECTIVES AND OVERVIEW

One of the central challenges in molecular biophysics is to understand how proteins control biochemical reactions in living organisms. In their folded states, proteins exhibit a variety of structural fluctuations. The question before us is; how do protein structure and dynamics control biological function? Our goal is to develop tools that allow us to simulate and understand those aspects of biomolecular structure and dynamics that establish the unique capabilities of these molecules. Our hope is to arrive at a deeper understanding of the mechanisms that control biochemical reactions and to establish design criteria for new proteins that will perform specific tasks.

With these issues in mind, this review focuses on electron transfer reactions. These reactions are extremely important in biology, particularly in bioenergetic reaction pathways (23, 32, 72). For example, in the early steps of photosynthesis, high efficiency solar-energy conversion is achieved with a complex of protein-bound electron donors and acceptors. Control of charge separation and recombination rates is required to insure that productive forward electron-transfer reactions within this complex occur rapidly, while wasteful back reactions occur orders of magnitude more slowly. Initial light-driven transfer steps are complete within 3 ps, and charge separation is subsequently stabilized for tens of milliseconds with a quantum efficiency near 100%. A comparable selective acceleration of electron transfer reactions has not been achieved in any artificial system.

Our goal in this paper is to present the results of a collaboration between theory and experiment aimed at developing a computational design capability for electron-transfer proteins. The theoretical methods we describe contain the minimal description that is needed to model adequately the fundamental mechanisms of protein-mediated electron tunneling. Although the description does not include every detail of the protein electronic structure, the model makes concrete, testable predictions about primary, secondary, tertiary, and quaternary structural effects on electron-transfer rates. Measurements of electron transfer rates in ruthenium-modified (ruthenated) proteins test the method's reliability. We find that

inclusion of protein features neglected in structureless barrier models is essential for understanding the observed transfer rates in these systems.

ELECTRON TUNNELING MATRIX ELEMENTS

This review focuses on the calculation of tunneling matrix elements (T_{DA}) and the comparison of these couplings with those derived from experiment (28, 38, 42, 51, 60). The tunneling matrix element is associated with the weak long-distance electronic coupling between donor (D) and acceptor (A) mediated by the protein. Electron-transfer rates in the proteins discussed here are in the nonadiabatic limit and are therefore proportional to T_{DA}^2. In this section, we present a short discussion of the dynamical limits associated with the nonadiabatic electron-transfer rate formulation. Special attention is given to the Hamiltonian that we use to describe our problem and why the nonadiabatic limit is appropriate for long-distance electron transfer in proteins.

We begin our discussion by presenting the Hamiltonian that has been used extensively for the generic electron transfer problem (12, 34, 52, 65, 67):

$$\mathscr{H}_{ET} = T_{DA}(Q)\sigma_x - \tfrac{1}{2}[\alpha_D^{eff}(Q)+\alpha_A^{eff}(Q)] + \tfrac{1}{2}[\alpha_D^{eff}(Q)-\alpha_A^{eff}(Q)]\sigma_z + \mathscr{H}_Q. \qquad 1.$$

The terms σ_x and σ_z are the Pauli matrices, where the expression $\sigma_z = 1$ or -1 is associated with the donor- or acceptor-localized state, respectively. $\mathscr{H}_Q$ supplies the dynamics for the nuclear coordinates (Q), and $\alpha_D^{eff}(Q)$ [$\alpha_A^{eff}(Q)$] is the instantaneous energy for the reactants (products) state.

Two major aspects of this Hamiltonian should be considered. First, it is necessary to describe why a multisite many-electron Hamiltonian can be reduced [renormalized to an effective two-level one-electron system (Equation 1)]. Second, if this renormalization is valid, we must present the conditions for the electron transfer rate to fall in the nonadiabatic limit (28, 51), i.e.

$$k_{ET} = \frac{2\pi}{\hbar} T_{DA}^2(FC), \qquad 2.$$

where (FC) is the nuclear (or Franck–Condon) factor. The analysis of experiments presented in this review relies on the separability of the rate expression.

Ideally, we would describe the molecular system from first principles including the motion of all the electrons and nuclei. Because this task is impossible, our strategy is to break the problem into pieces that can be

understood. To be successful, such a simplification relies on the identification of the relevant energy scales of the problem.

Before addressing the details of the molecular electronic structure, we assume that the Born-Oppenheimer approximation is valid. This assumption is appropriate if the energies for nuclear excitations are much smaller than those for electronic excitations. We comment later about the important excitations in the electron-tunneling problem and why we believe this assumption is valid. The electronic energies of chemical bonds are much smaller than the electronic excitation energies of core electrons. We can therefore describe our problem as valence electrons moving in a pseudopotential provided by the core electrons and nuclei. Actually, we can expand this picture by assuming that the energy associated with electronic coupling between atoms (or bonds) is small compared to the energy of excited states on isolated atoms, leading to a tight-binding or extended-Hückel picture (for details, see 6, 10, 12, 58).

The initial tight-binding electronic Hamiltonian for D, A, and their bridge is written (4, 6, 12, 27, 47, 48, 58, 59, 63, 64, 66, 70, 71):

$$\mathscr{H}_{el} = \alpha_D a_D^\dagger a_D + \alpha_A a_A^\dagger a_A + \sum_{i_D} v_{D,i_D}(a_D^\dagger a_{i_D} + a_{i_D}^\dagger a_D) + \sum_{i_A} v_{A,i_A}(a_A^\dagger a_{i_A} + a_{i_A}^\dagger a_A) + \sum_i \alpha_i a_i^\dagger a_i + \sum_{i,j>i} v_{ij}(a_i^\dagger a_j + a_j^\dagger a_i), \quad 3.$$

where the $a_\mu^\dagger$ (a_μ) creates (destroys) an electron on the μth orbital. The first two terms in the Hamiltonian represent the donor and acceptor sites. The third and fourth terms contain the coupling between the donor and acceptor, respectively, and the bridge. Bridge orbitals coupled to the donor and acceptor are labeled i_D and i_A, respectively. The last two terms are the bridge Hamiltonian. Because we are using the Born-Oppenheimer approximation, all the electronic energies (α and v) are a function of the nuclear configuration **Q**.

How do we reduce the above Hamiltonian (Equation 3) to a two-level system (reactants and products)? One way is to use the Löwdin partitioning technique (47, 59). With this method, one maps an eigenvalue problem of high dimension onto an equivalent problem of lower dimension. The Hamiltonian or Equation 3 in matrix notation is:

$$\begin{pmatrix} \mathscr{H}_{DA} & \mathscr{H}_{DA,B} \\ \mathscr{H}_{B,DA} & \mathscr{H}_{bridge} \end{pmatrix}, \quad 4.$$

where $\mathscr{H}_{DA}$ is the matrix Hamiltonian that only includes the donor and acceptor sites. The direct coupling between D and A in the case of long-distance transfer is negligible. $\mathscr{H}_{bridge}$ is the Hamiltonian matrix for the bridge, and $\mathscr{H}_{B,DA}$ is the matrix that couples the donor and acceptor to the bridge. Löwdin diagonalization yields a reduced 2 × 2 matrix

$$\bar{\mathscr{H}}_{DA} = \mathscr{H}_{DA} - \mathscr{H}_{DA,B}\mathscr{H}_{bridge}^{-1}\mathscr{H}_{B,DA}. \quad 5.$$

The effective matrix one obtains is

$$\bar{\mathscr{H}}_{DA} = \begin{bmatrix} \alpha_D^{eff}(E) & T_{DA}(E) \\ T_{AD}(E) & \alpha_A^{eff}(E) \end{bmatrix}, \quad 6a.$$

where

$$\alpha_{D(A)}^{eff}(E) = \alpha_{D(A)} + \Delta_{D(A)}(E), \quad 6b.$$

$$\Delta_{D(A)} = \sum_{i,j} v_{D(A)i} G_{ij}(E) v_{jD(A)}, \quad 6c.$$

and

$$T_{DA} = \sum_{i,j} v_{Di} G_{ij}(E) v_{jA}. \quad 6d.$$

The *i*s and *j*s in the sums run over the bridge orbitals. G is the Green's function for the bridge, i.e. the Green's function (7, 25, 26, 35, 50, 52, 66, 67a) associated with $\mathscr{H}_{el}$ without the donor and acceptor terms, $G = (\mathscr{H}_{bridge} - E)^{-1}$.

Equation 6 is equivalent to Equation 5, i.e. the eigenvalues for the two equations are the same. However, we are only interested in the two states that define the two-level system. The first step in analyzing these states is to determine the tunneling energy. The effective donor energy can be obtained from Equation 6 by solving

$$\bar{\alpha}_D = \alpha_D^{eff}(\bar{\alpha}_D). \quad 7.$$

The root of this equation closest to α_D is the effective donor energy. This result is equivalent to the one used in our laboratory (see 4, 65, for example) when considering the isolated donor-plus-bridge system. A similar calculation can be performed for the acceptor. The tunneling energy, E_T, is obtained for the nuclear configuration **Q** where

$$E_T = \bar{\alpha}_D = \bar{\alpha}_A. \quad 8.$$

After calculating the tunneling energy, we can finally obtain the two-level system by fixing the value of E in Equation 6 equal to E_T. How good is this approximation? Let us refer to the symmetric and antisymmetric state energies that define the two-level system as E_1 and E_2, respectively. $E_2 - E_1$ is twice the tunneling matrix element. E_T is exactly midway between E_2 and E_1. Therefore, if we compare E_2 and E_1 as the eigenvalues of

Equation 6, setting $E = E_T$, we introduce errors of the order $E_2 - E_1$. Because E in Equation 6 only appears in terms like $\alpha_i - E$, the error introduced is approximately $(T_{DA}/|\alpha_{bridge} - E_T|)$. This error is of the order of the overlap between the effective donor and the acceptor states.

In order for the two-level approximation to hold, the separation between levels one and two, $2T_{DA}$, must be small compared to the energy separation between these states and the bridge. Actually, the ratio of these two quantities determines the precision of the approximation. Also, for the Born-Oppenheimer approximation to hold, these energy separations must be large compared to any relevant nuclear excitation energies. Finally, for this approximation to be valid, the investigator must consider one more time (energy) scale. As the electron tunnels from the donor to the acceptor, it spends a certain time in the classically forbidden region (12, 18). If this time is much shorter than the period of the vibrational modes, the atoms stay fixed as the electron tunnels; in other words, the Born-Oppenheimer approximation works. These approximations are reasonably good for electron transfer in proteins, and the reader is referred elsewhere (5, 12, 65) for further details.

To conclude this section, we comment on the nonadiabatic approximation that leads to an electron-transfer rate given by Equation 2. In order for this limit to be valid, the electronic frequency, T_{DA}/h, must be low compared to that of the relevant nuclear motion. In the past six years, many papers have addressed this subject (see 67 and references therein for details). In long-distance electron transfer, the tunneling matrix elements are so small that this approximation most likely is adequate.

THE PATHWAY MODEL

The pathway model of electronic coupling in proteins (3, 6, 7, 8, 11) was developed based on earlier studies of electronic coupling in model compounds (4, 7, 63). Tunneling is much more efficient (decays more slowly) through bonded orbitals than through space, because the potential barrier is effectively lower. In proteins, the bonded-path connection length between D and A can be extremely long compared with the direct through-space distance. Our pathway method searches for the combination of bonded and nonbonded interactions that maximizes the total D-A interaction mediated by a combination of through-bond and through-space coupling through the protein. The tunneling pathways obtained contain mostly bonded interactions (with occasional through-space connections).

The intervening protein could provide two distinct mediation mechanisms to couple D and A. One mechanism mediates the interaction by a few very specific combinations of interacting bonds (fragments of amino acids) between D and A. The bonds would couple D and A through a sequence of directly connected covalent bonds, hydrogen bonds, and noncovalent contacts. Each of these combinations is called a *physical tunneling pathway* and plays a role in the D-A coupling (8). The other distinct way that the protein might couple D and A involves a sufficiently large number of pathways such that modifying a single pathway in this network will have a very small effect on the net coupling and the rate. In this case, no particular detail of the protein will greatly affect the rate.

An elaboration of the discussion of a physical tunneling pathway can help us focus the discussion of the D-A coupling mechanism. For a single physical pathway, one can use exact and perturbation theory methods for calculating the coupling arising from that physical pathway. Numerical strategies (for both exact and perturbation methods) usually write the decay of the wave function as a product of decays per bond [or delocalized group (63, 64)]. Within a lowest-order perturbation theory calculation, the per-bond decay depends only on the tunneling energy and on the nature of the particular bonds in the pathway. This method (applied to lowest order) neglects scattering corrections to the wave function propagation in the protein bridge. The scattering corrections (equivalent to higher-order perturbation-theory corrections) for a given pathway arise from enumerations of bonds in the tunneling pathway longer than the shortest path from D to A. For example, a physical pathway consisting of bonds 1, 2, 3, 4, . . . has the direct pathway 1-2-3-4 . . . and the scattering pathways 1-2-3-2-3-4 . . . , etc. We now discuss how one can exactly account for the scattering pathways in the electronic-coupling calculation for a one-dimensional physical pathway by correcting the self energy of each orbital on the path. Exact methods, particularly Green's function approaches, often write the coupling as a product as well. In this case, the terms in the product explicitly include these scattering corrections. In the same way, the effect of side groups appended to the physical pathway can also be included.

For a single physical pathway, the tunneling matrix element can be written (7, 53)

$$t_{DA} = \text{prefactor} \prod_{i=1}^{N} \varepsilon_i. \qquad 9.$$

Neglecting interactions between pathways within the protein bridge, T_{DA} is a sum over t_{DA}s for all physical pathways. For a pathway, ε_i for each block in the path (66) may be calculated approximately or exactly as discussed above. The prefactor depends on details of the interaction between the D or A with the first or last, respectively, bond of the tunneling

pathway. When experimental systems with similar (or properly scaled) prefactors and *FC* factors are compared, differences in electron-transfer rates are expected to result from differences in the coupling via the physical pathways of the systems. The challenge in proteins, then, is to identify the chains of orbitals that define dominant pathways. The dominant tunneling pathways correspond to the combinations of bonds in the protein that maximize the products in Equation 9.

As an example of how to compute ε_i, we consider a linear chain of identical (Figure 1*a*) orbitals coupling the donor and the acceptor. (The orbital energy is α_B and the coupling between neighbors is v.) If backscattering is neglected, the decay per orbital is

$$\varepsilon = v/(E_I - \alpha_B), \qquad 10.$$

where v is the coupling between neighboring bridge orbitals, and α is the orbital energy. The exact result, including backscattering, can also be written as the product given by Equation 9. The decay ε_i between bonds i and $i+1$ is:

$$\varepsilon_i(E_I) = \frac{G^{j}_{1,j+1}}{G^{j}_{1,j}} = \frac{v}{E_I - (\alpha_B + \delta_i^{bs})}, \qquad 11.$$

where δ_i^{bs} is the site self-energy correction due to backscattering. G^j is the Green's function for a linear bridge of j orbitals. In the long chain limit ($i \gg 1$), this result converges to the infinite-chain limit

$$\varepsilon^{\infty}_{exact}(E) + \frac{1}{\varepsilon^{\infty}_{exact}(E)} = \frac{E - \alpha_B}{v}. \qquad 12.$$

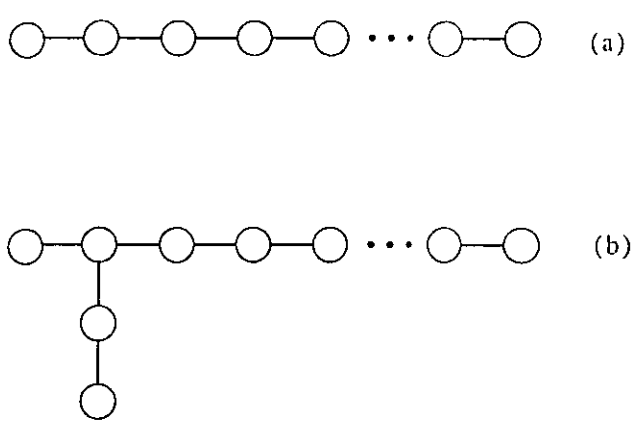

Figure 1 (*a*) Schematic representation of a linear bridge. Only nearest neighbors are coupled. (*b*) Schematic representation of a side group coupled to an orbital in the pathway.

We refer the reader elsewhere (66) for details about how these Green's functions can be calculated and for a description of our stepwise Green's function method.

The effect of pendant (side) groups can also be included without destroying the pathway concept. This concept is associated with the possibility of writing t_{DA} as a product of εs. Figure 1*b* suggests that pathways can include the effects of side groups attached to a single site by modifying the self energy of the orbital that the pendant group is attached to. Assuming that the side chain is coupled to pathway orbital i via orbital $s1$, the side chain can be eliminated by renormalizing the orbital i energy:

$$\alpha_i^{eff} = \alpha_i + v_{i,s1} G^{sc}_{s1,s1} v_{s1,i}. \qquad 13.$$

$G^{sc}_{s1,s1}$ is the diagonal matrix element of the Green's function for site $s1$ when only the side chain is included in the Hamiltonian. Using this procedure, many side chains can be immediately eliminated at the early stages of the calculation, greatly simplifying the problem.

The validity of the pathway approximation only becomes suspect when loops involving several paths appear. If interference between pathways is considerable, contributions from independent pathways enter T_{DA} in a rather complex manner. To address this issue, we developed a stepwise Green's function technique, and research is underway to understand the general applicability of the pathway concept. The simple pathway concept without the inclusion of effects like those discussed above can still teach us much about the mediation of electron tunneling in proteins.

Our strategy for mapping tunneling pathways in proteins involves making approximations to the decay factors ε_i and performing computer searches for the combination of interacting bonds with decay factors that maximize the product in Equation 9.

PATHWAY SEARCH STRATEGIES

The Conceptual Basis of the Calculations

The single maximum coupling pathway between two points in a protein indicates, at the very least, the coupling strength between those regions of the molecule. This section describes our simple approximations (based on intuition gained from model compound studies) used to produce a computationally tractable approximation to the coupling given in Equation 9 in which a product of decay factors give the contribution to T_{DA} from a single pathway. Our ansatz partitions electronic mediation through protein into three types of interactions: covalent, hydrogen-bonded, and through-space. This division was based on the fact that bond-mediated interactions are much longer range than through-space interactions (7).

The barrier to tunneling through a bonded medium is considerably lower than tunneling through vacuum (6, 10, 11) so the exponential decay of bond-mediated coupling is slower than through-space tunneling. Hydrogen bonds are weaker than covalent bonds, so it was not immediately apparent that they would be key mediators of tunneling. However, because hydrogen bonds bring lone-pair and bonding orbitals into close proximity, we expect their mediation properties to be substantial (8, 64).

Bonded and nonbonded interaction energies are obviously a function of atom type, hybridization, and orientation. However, the distinction between bonded and nonbonded interactions is so strong that a preliminary understanding of coupling pathways arises from determining the mix of these interactions on the dominant routes. For a single pathway consisting of covalent (C), hydrogen-bonded (H), and through-space (S) interactions, Equation 9 can be rewritten:

$$T_{DA} \propto \prod_i \varepsilon_C(i) \prod_j \varepsilon_S(j) \prod_k \varepsilon_H(k). \qquad 14.$$

Because the rate of electron transfer (Equation 2) is proportional to T_{DA}^2, we can estimate relative rates from Equation 14 for a given nuclear FC factor. By writing the T_{DA} expression with a proportionality, we have suppressed prefactors associated with D-bridge and bridge-A coupling. These factors have been discussed elsewhere (22, 64) and for the purposes of this discussion are assumed to be the same for all pathways. Simpler models for electron tunneling in proteins would write T_{DA} (and the transfer rate) as proportional to an exponentially decaying factor arising from a simple one-dimensional square barrier (28):

$$k_{ET}(\text{square}) = A \exp(-\beta R)(FC). \qquad 15.$$

The goal of the algorithm described in the next section is to find the combination of bonds between D and A that maximizes the product in Equation 14 given simple rules for approximating the decay factors ε. Other theoretical strategies for calculating the tunneling matrix element are also being developed (14, 19, 46).

Coupling Decay Factors

We now consider the range of decay parameters that are chemically accessible and describe the computer-search strategy for finding pathways that maximize the product in Equation 14 for a set of specified decay factors. Many covalently coupled D-A model compounds that undergo photoinduced electron transfer have been constructed with both biological and nonbiological redox active chromophores. When one translates the reported decays of rate with bridge size to decay per bond factors of the tunneling matrix element, through-bond ε_C decay factors are calculated in the range ~0.7–0.4 (55). We have chosen a value of 0.6 because it is a reasonable average value for the decay per bond (see 64 for details). Although ratios of rates depend on the choice, if all ε_Cs are assumed to be the same, the qualitative results of the single pathway calculations are insensitive to the exact value chosen (because ε_C appears as a prefactor in all three terms). The key relationship is between ε_C and the through-space decay constant. Through-space interactions are treated as stretched bonds, with couplings that are weaker than the bonded couplings by an amount commensurate with the length of the interaction beyond the reference covalent-bond length. An additional factor, usually taken as 1/2, is added to account for the generally unfavorable orientation effects associated with through-space interactions. The decay length, 1.7 $Å^{-1}$ for the through-space interaction, arises from the calculation of penetration through a one-dimensional square barrier, which drops with exponential decay constant $(2m_e E_B/h^2)^{1/2}$, where m_e is the electron mass and E_B is the tunneling electron energy, about 10 eV (11). Tunneling energies chosen in the 5–10 eV range have been explored. Again, the results are insensitive to the specific value. The hydrogen-bond decay is treated as two covalent bonds from heteroatom to heteroatom, allowing one to adjust the coupling if the bond length is longer or shorter than the reference length. Thus, we have arrived at the following parameter set (8, 9):

$$\varepsilon_C = 0.6 \qquad 16a.$$

$$\varepsilon_H = \varepsilon_C^2 \exp[-1.7(R-2.8)] \qquad 16b.$$

$$\varepsilon_S = (1/2)\varepsilon_C \exp[-1.7(R-1.4)]. \qquad 16c.$$

In these expressions, the distances, R, are in Å units and the decay factors, ε, are unitless. The reference covalent bond distance is chosen as 1.4 Å (2.8 Å for two bonds). These decay factors include the minimal amount of physical detail needed to understand the structural dependence of electronic coupling in a bridge. As such, they provide a starting point for the development of structure-function relationships that, if promising, will be elaborated to include numerous fascinating complications arising from quantum interference within and between pathways, bond energetic differences, and geometric fluctuations from assumed atomic positions, to name a few.

Finding the Best Path

How are the pathway searches actually performed? These parameters are consistent with typical binding energies for electron-transfer localized

states as well as theoretical and experimental studies of model compounds (9). Each decay factor ε is associated with an effective distance d_{eff} where:

$$d_{\text{eff}}(i) = -\log \varepsilon(i). \qquad 17.$$

We refer both to decay factors and connection lengths throughout the paper. The strength of the coupling arising from a single (noninterfering) pathway is proportional to the product of decay factors for each step on the path: $\Pi_i \varepsilon_i$. The computational challenge is to analyze the highly interconnected network of bonded and nonbonded contacts in a protein and specify the bonds that maximize this product. This is precisely the well-known minimum-distance-in-a-graph problem. The minimum-distance problem addresses finding the shortest pathway between two points in an interconnected network. Because Equation 17 associates the decay factor with an effective distance, we can restate our search for the maximum pathway couplings as a search for the shortest effective distance between donor and acceptor in the corresponding network. Graph-theory strategies for solving the minimum-distance problem are discussed elsewhere (17).

The first step in using graph theory to find electron-transfer pathways in proteins is to construct a labeled graph (17) corresponding to the superset of all potential pathways. Covalent bonds (established as described below) are first mapped onto vertices. Establishing which vertices are to be joined by edges requires progressively more computation for adjacent covalent bonds, hydrogen bonds, and through-space contacts. The lengths of the edges (i.e. the decays) are determined by the distances between the atoms and the nature of the interaction (Equation 16). The covalent bonds are specified implicitly by the Brookhaven Protein Data Bank files. Covalent interactions, those between bonds anchored at a common atom, are easily identified. Commercial software is used to look up these connections for the known amino acids and other residues, which are then appended to the Protein Data Bank data. These amended Protein Data Bank files are used as input to the PATHWAYS software written by J. N. Betts. Directed by data in the parameter files, the program looks up the model-predicted decays (Equation 16) for the various bond types and stores them. Hydrogen bonds are identified as having acceptable: (*a*) hydrogen-donor and hydrogen-acceptor groups (donors: -NHx; acceptors: carbonyl oxygens; both: -OH), (*b*) donor-hydrogen-acceptor angle, and (*c*) donor-acceptor distance (Å). These values are specified in a parameter file. Edges representing the hydrogen bonds are added to the connection list, and lengths that represent these decays are added to the list of segment lengths. Next, potential through-space connections are sought within a limited radius of each atom, typically 6 Å. No through-space connections longer than 6 Å contribute to significant pathways, so they are ignored

to shorten the data-processing time. The through-space connections are established for each atom, X, as follows. First, the investigator composes a list, L, containing all bonds/vertices within range of X and attempts to eliminate as many of the entries as possible. Through-space connections are eliminated between atoms that have a significantly stronger bond-mediated connection. The first through-space connections the program eliminates from L are those that are redundant with preexisting covalent and hydrogen bonds. The vertices remaining in L are sorted on the basis of their distances from X, shortest first. Next, a depth-first shortest-path search (17) is performed with X as the root, finding the shortest distance to atoms with potential through-space connections. The depth of the search is limited to a length that corresponds to the through-space decay from X to atoms within the through-space cutoff radius. If the search returns without having located the potential atom, the through-space contact is the shortest path to it, and the connection is thus added to the master connection (adjacency) list, and its corresponding length is added to the list of lengths. Otherwise, the through-space connection is discarded and the next vertex in L becomes the new target. In this way, shorter through-space contacts can disqualify longer ones, further decreasing the number of connections added to the graph.

Two standard search strategies are used to arrive at the minimum-distance path between two points in an interconnected network, referred to as depth-first and breadth-first searches. Depth-first searches begin at a specified point and step along allowed connections until no additional forward steps remain (a dead-end is reached) or the target site is found. If a dead-end occurs, the search backtracks by one step and then seeks alternative forward steps from that point, and so on until the target atom is found. Breadth-first searches simultaneously consider all paths radiating from the starting point by keeping track of each vertex and its distance. At each step of the search, a new vertex is added. The vertex chosen to be added is always the one that minimizes the effective distance to the donor at that stage. When the acceptor atom is the one that is added, the minimum-distance pathway has been found. We use a depth-first algorithm. The advantage of the depth-first search for our applications is its pathway orientation, i.e. each excursion represents a potentially acceptable pathway and the paths within a given factor of the best pathway are easily tabulated and accumulated.

RUTHENATED CYTOCHROMES

The molecules we have employed in experiments aimed at extracting T_{DA} values are ones in which ruthenium complexes are attached to surface

histidines of structurally characterized proteins (2, 13, 22, 24, 30, 36, 40, 41, 44, 45, 49, 54, 61, 68, 73, 74, 74a, 75, 77–79). Surface modification of a protein is expected to be nonperturbative, so the structure of the modified protein is presumably the same as that of the native protein. Hence, the distance and the intervening medium involved in electron transfer between the native- and synthetic-protein redox sites are known. Altering the site of attachment allows one to vary both the distance and the intervening medium for electron transfer. Changing the ligands in the ruthenium modification reagent also permits one to study free-energy effects on the rate of the reaction.

Cytochrome c

HIS33 DERIVATIVES The first experimental work on the electron-transfer reactions of Ru-modified proteins involved horse-heart cytochrome *c* modified by coordination of pentaammineruthenium to His33 (Figure 2) (75, 77). The rate of intramolecular electron transfer from $Ru a_5(His33)^{2+}$ ($a = NH_3$) to the ferriheme ($T = 298$ K), measured using photochemical techniques, is $30(\pm 5)\ s^{-1}$ (Table 1). The reaction exhibits a rather small activation enthalpy (2 kcal mol^{-1}) and a large negative activation entropy (−43 eu). Measurements of the temperature dependences of the $Ru a_5(His)^{3+/2+}$ and $Fe^{3+/2+}$ potentials in $Ru a_5$(His33)-Fe-cyt *c* have provided estimates of ΔG° [$-4.3(\pm 2)$ kcal mol^{-1}, 298 K), ΔH° [$-11.5(\pm 10)$ kcal mol^{-1}], and ΔS° [$-25(\pm 3)$ eu] for the Ru(II)Fe(III) intramolecular electron-transfer reaction. Given these thermodynamic quantities, and the temperature dependence (2–40°C) of the electron-transfer rate in $Ru a_5$(His33)-Fe-cyt *c*, one can extract values of λ and T_{DA} from Equation 2 using a classical expression for *FC* (51). Nonlinear least-square fits to the data suggest that $\lambda = 1.2$ eV and $T_{DA} = 0.03$ cm $^{-1}$ (74a). This value of the reorganization energy is quite close to that predicted by the Marcus cross relation (59) [$\lambda_{12} = (\lambda_1 + \lambda_2)/2$] using the reorganization energies for the Fe-cyt *c* ($\lambda_{11} = 1.04$ eV) and $Ru a_5(py)^{3+/2+}$ ($\lambda_{22} = 1.20$ eV) self-exchange reactions (15, 51).

A clear understanding of the electronic-coupling strengths in metalloprotein electron-transfer reactions depends upon reliable values of λ and T_{DA}. In addition to studies of temperature dependences, analysis of the driving-force dependence of electron transfer rates can also provide electron-transfer parameters. In the low-driving-force regime ($-\Delta G^\circ \ll \lambda$), the variation of rate with free energy does not strongly depend upon λ, and it is difficult to obtain a good value for this parameter. Much better values of λ and T_{DA} can be obtained from high-driving-force measurements (i.e. $-\Delta G^\circ \approx \lambda$). In this region, the driving-force curve flattens out and electron-transfer rates approach their maximum values.

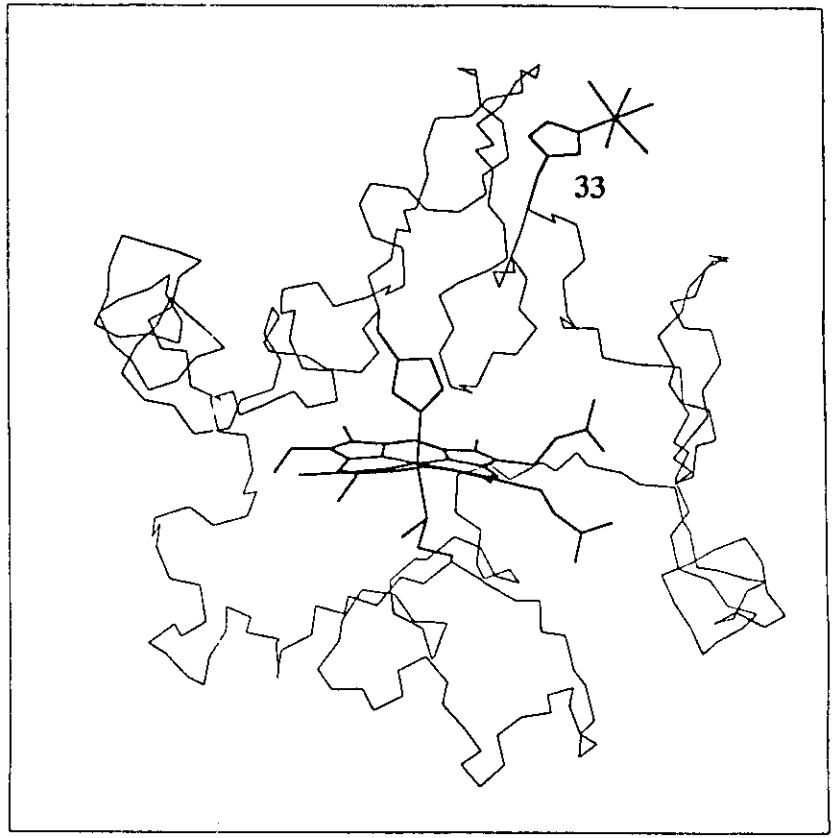

Figure 2 Peptide-backbone structure of $Ru a_5$(His33)-Fe-cyt *c*. This complex was prepared by reaction of $Ru a_5(OH_2)^{2+}$ with Fe(II)-cyt *c* for 24 h at room temperature. The pure singly modified derivative was isolated using ion-exchange chromatography and was extensively characterized by spectroscopic and chemical methods (77, 78).

It is difficult to prepare a Ru-ammine complex of Fe-cyt *c* in which the driving force for intramolecular electron transfer is much greater than 0.2 eV. Substitution of the native Fe center in cytochrome *c* with Zn, however, has led to high-driving-force intramolecular electron transfer. The lowest triplet-excited state of the Zn-porphyrin in Zn-cyt *c* has a 15-ms lifetime and is a potent reductant [$E^\circ = -0.62$ V vs normal hydrogen electrode (NHE)]. The rates of direct photoinduced electron transfer and thermal recombination have been measured for three $Ru a_5$L(His33)-Zn-cyt *c* proteins (L = NH_3, pyridine, isonicotinamide), spanning a 0.39-eV range in ΔG° (−0.66 to −1.05 eV; Table 1) (30, 54, 74). Fits of these data yield

Table 1 Rate constants and activation parameters for intramolecular electron-transfer reactions of Ru(His)-modified cytochrome *c*

Electron transfer	$-\Delta G^\circ$ (eV)	k_{ET} (s^{-1})	$\Delta H^\ddagger$ (kcal mol^{-1})	$\Delta S^\ddagger$ (eu)
His33 Derivatives (d = 11.1 Å)				
$Ru_5(His)^{2+} \rightarrow Fe(III)^a$	0.18(2)	$3.0(5) \times 10^1$	2.0(5)	−4.7(5)
$Ru_4(isn)(His)^{2+} \rightarrow ZnP^{+b}$	0.66(5)	$2.0(2) \times 10^5$	<0.5	−3.1(5)
$ZnP^* \rightarrow Ru_5(His)^{3+c}$	0.70(5)	$7.7(8) \times 10^5$	1.7(4)	−2.1(5)
$Ru_4(py)(His)^{2+} \rightarrow ZnP^{+b}$	0.74(5)	$3.5(4) \times 10^5$	<0.5	−3.2(5)
$ZnP^* \rightarrow Ru_4(py)(His)^{3+b}$	0.97(5)	$3.3(3) \times 10^6$	2.2(4)	−2.1(5)
$Ru_5(His)^{2+} \rightarrow ZnP^{+c}$	1.01(5)	$1.6(4) \times 10^6$	—	—
$ZnP^* \rightarrow Ru_4(isn)(His)^{3+b}$	1.05(5)	$2.9(3) \times 10^6$	<0.5	−30(5)
His39 Derivatives (d = 12.3 Å)[d]				
$Ru_4(isn)(His)^{2+} \rightarrow ZnP^+$	0.66(5)	$6.5(7) \times 10^5$	−1.7(4)	−39(5)
$ZnP^* \rightarrow Ru_5(His)^{3+}$	0.70(5)	$1.5(2) \times 10^6$	1.3(3)	−27(5)
$Ru_4(py)(His)^{2+} \rightarrow ZnP^+$	0.74(5)	$1.5(2) \times 10^6$	−1.8(4)	−37(5)
$ZnP^* \rightarrow Ru_4(py)(His)^{3+}$	0.97(5)	$8.9(9) \times 10^6$	0.2(2)	−2.1(5)
$Ru_5(His)^{2+} \rightarrow ZnP^+$	1.01(5)	$5.7(6) \times 10^6$	−0.2(2)	−29(5)
$ZnP^* \rightarrow Ru_4(isn)(His)^{3+}$	1.05(5)	$1.0(1) \times 10^7$	0.2(2)	−27(5)
His62 Derivatives (d = 14.8 Å)[e]				
$ZnP^* \rightarrow Ru_5(His)^{3+}$	0.70(5)	$6.5(7) \times 10^1$	1.4(3)	−37(5)
$Ru_4(py)(His)^{2+} \rightarrow ZnP^+$	0.74(5)	$8.1(8) \times 10^1$	—	—
$ZnP^* \rightarrow Ru_4(py)(His)^{3+}$	0.97(5)	$3.6(4) \times 10^3$	—	—
$Ru_5(His)^{2+} \rightarrow ZnP^+$	1.01(5)	$2.0(2) \times 10^4$	0.7(7)	−37(5)

[a] References 61, 75.
[b] Reference 54.
[c] Reference 30.
[d] Reference 74.
[e] Reference 73.

$\lambda = 1.10$ eV and $T_{DA} = 0.12$ cm^{-1} for the photoinduced reactions, and $\lambda = 1.19$ eV and $T_{DA} = 0.09$ cm^{-1} for the recombinations. The electron-transfer parameters are not extremely sensitive to the nature of the reaction (photoinduced or recombination), and these reactions can be adequately described by a single pair of parameters: $\lambda = 1.15(10)$ eV and $T_{DA} = 0.1(2)$ cm^{-1} (74a).

The similarity in reorganization energies for the Ru-Fe-cyt *c* and Ru-Zn-cyt *c* intramolecular electron-transfer reactions is to be expected. The total reorganization energy is a sum of inner-sphere (λ_i) and outer-sphere (λ_o) elements. Inner-sphere contributions arise from nuclear rearrangements in the Ru-ammine and metalloporphyrin complexes accompanying electron transfer. These rearrangements are rather small and have been estimated to contribute no more than 0.2 eV to λ for both Ru-Fe-cyt *c* and Ru-Zn-cyt *c* (54). The two sources of outer-sphere rearrangements are the solvent and the peptide matrix. Calculations based on a single-sphere dielectric continuum model (16) indicate a 0.6-eV contribution to λ_o from the solvent (54). From the structures of ferri- and ferrocytochrome *c*s, the peptide contribution to λ_o has been calculated to be about 0.2 eV (20). The sum of these individual components (1.0 eV) is in good agreement with the experimentally derived reorganization energy for the Ru-M-cyt *c* (M = Fe, Zn) systems.

HIS39 DERIVATIVES Ru-ammine complexes have been bound to His39 of Zn-substituted cytochrome *c* from *Candida krusei* (68, 74). Intramolecular electron-transfer rates (Table 1) are approximately three times faster than those of corresponding reactions in His33 derivatives of horse-heart cytochrome *c*. The variation of rates with driving force in these derivatives suggests a 1.2(1) eV reorganization energy, indistinguishable from that found in the His33 complexes. The faster electron-transfer rates have been attributed to stronger donor-acceptor electronic coupling in the His39-modified protein (74).

The direct D-A distances in Ru(His33)-Zn-cyt *c* and Ru(His39)-Zn-cyt *c* are 11.1 and 12.3 Å, respectively; however, the T_{DA} is twofold larger for the His39 system. The pathway model is somewhat more consistent with the data: both the His33 and His39 pathways consist of 11 covalent bonds and 1 hydrogen bond (Figure 3). The n_{eff} values for His33 and His39 are 13.9 and 14.0 bonds, respectively (74a).

HIS62 DERIVATIVES Site-directed mutagenesis creates many new opportunities for studying electron transfer in Ru-modified proteins. A yeast (*Saccharomyces cerevisiae*) cytochrome *c* variant has been characterized as having a surface histidine at position 62 (13). The Ru_5(His62) derivative of this mutant protein was prepared, and the rate of electron transfer from Ru(II) to Fe(III) was found to be 1.7 s^{-1} (Table 1) (13). Ru_5(His62) and Ru_4(His62) derivatives of Zn-substituted *S. cerevisiae* cytochrome *c* have also been examined. The rates of the photoinduced and thermal recombination reactions are more than two orders of magnitude slower than the rates of analogous reactions in His33 derivatives of horse-heart cytochrome *c* (73). The driving-force data are more limited than for the other His derivatives of cytochrome *c*, but again suggest that $\lambda \approx 1.2$ eV. The slower rates for the His62 derivatives are attributed to weaker electronic coupling. The direct D-A separation is 14.8 Å, while the effective number of bonds in the pathway is 20.6 (Figure 3) (74a). Both measures suggest that the His62 electron transfer reactions should be substantially slower than those found in His33 or His39 derivatives.

NATURE OF THE PATHWAYS Qualitative differences can arise in the collection of best pathways found, depending on the protein structure. We have

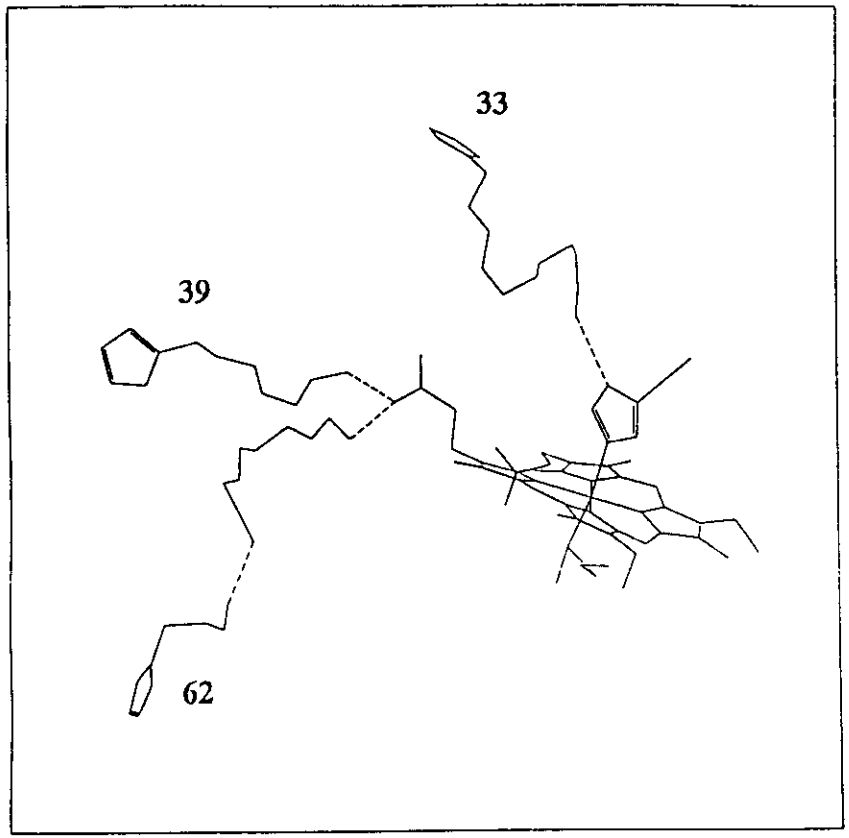

Figure 3 Predicted electronic-coupling pathways in Ru(His33)-, Ru(His39)-, and Ru(His62)-modified cytochrome *c*. Covalent bonds are depicted as solid lines and hydrogen bonds as dashed lines.

examined the paths within a factor of 10 of the best one in ruthenated His39 and His62 cytochrome *c*. In the His39 derivative, three routes feed into a single propionic acid side chain of the heme (Figure 4). The three pathways are more or less parallel and not highly interconnected. His62 has only two classes of pathways, but paths between and within each class have intertwined pathways near the His62 group, which are independent at intermediate distance and connect to independent parts of the heme. Pathway coupling calculations can be displayed in map form: Figure 5 is a coupling map showing the maximum pathway coupling to each α-carbon in cytochrome *c*.

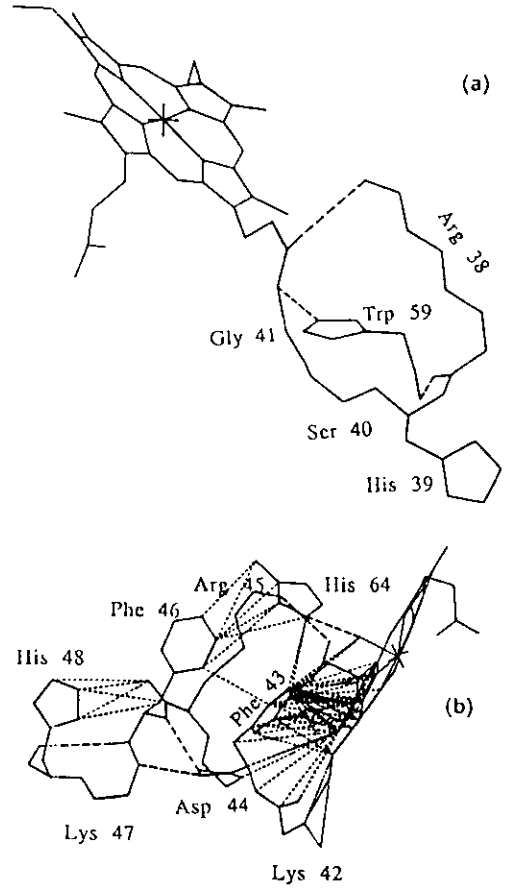

Figure 4 The best paths for (*a*) His39 cyt *c* and (*b*) His48 Mb are shown. Dotted lines are through-space contacts. Note that the best paths in cyt *c* are structurally related to one another, while several classes of pathways exist in Mb.

Cytochrome b_5

HIS26 DERIVATIVES Three surface His residues of trypsin-solubilized bovine cytochrome b_5 (Tb_5) have been modified by coordination to Ru-penta-ammine complexes (His15, His80, His26) (40). Rates of intramolecular electron transfer from Fe(II) to Ru(III) have been measured in three His26 derivatives: Rua_5(His26)-Tb_5; mutant (Asn57 to Asp, Gln13 to Glu, Glu11 to Gln, His15 to Asn, His80 to Asn) lipase-solubilized cytochrome b_5 [Rua_5(His26)LMb_5]; and deuteroporphyrin-substituted (DP) Tb_5 [Rua_5(His26)DPb_5] (40, 41). Electron-transfer rates vary by more than an

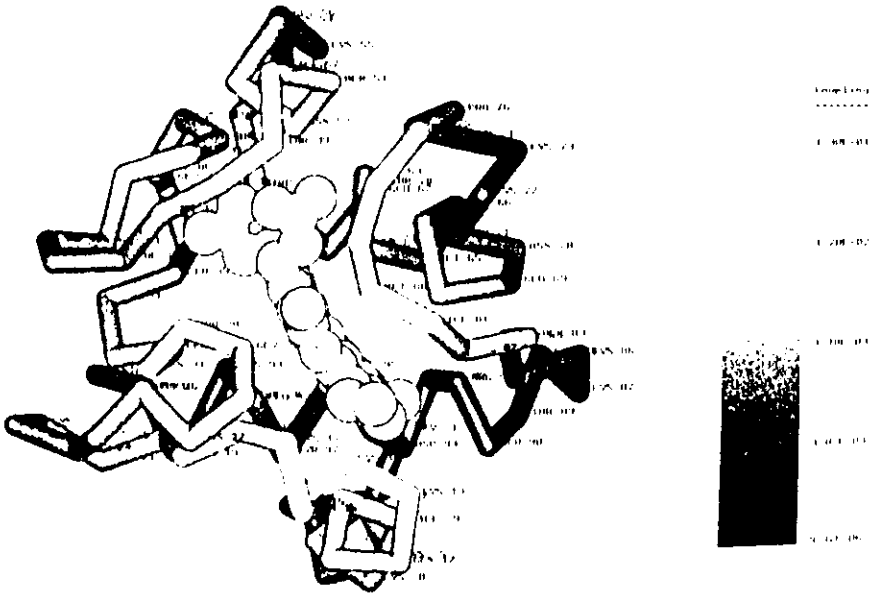

Figure 5 Electronic coupling map for cytochrome *c*. Amino acids directly connected to those coordinating the Fe or hydrogen-bonding to the heme are anomalously strongly coupled in reference to their through-space distance from the heme.

order of magnitude for the three proteins (Table 2). The small differences in driving force or estimated D-A separation cannot readily account for the variations in rate. Driving-force data are not available for this system, but changes in λ probably could not be responsible for the differences in electron-transfer rates. The pathway model has been invoked to account for the differences in rates. A critical through-space jump (from Leu25 to the heme) in the pathway from His26 to the heme is not constant in the three different proteins (Figure 6). The dramatic reduction in rate in Rua_5(His26)DPb_5 has been attributed to the absence of the heme 2-vinyl

Table 2 Electron-transfer rates in Ru(His26)-modified cytochrome b_5[a]

Electron transfer	$-\Delta G^\circ$ (eV)	k_{ET} (s^{-1})	d (Å)
Fe(II)-Tb_5 → Rua_5(His26)$^{3+}$	0.08(2)	1.4(1)	12.1
Fe(II)-LMb_5 → Rua_5(His26)$^{3+}$	0.10(2)	5.9(5)	12.0
Fe(II)-DPb_5 → Rua_5(His26)$^{3+}$	0.13(2)	0.2(1)	12.9

[a] Reference 41.

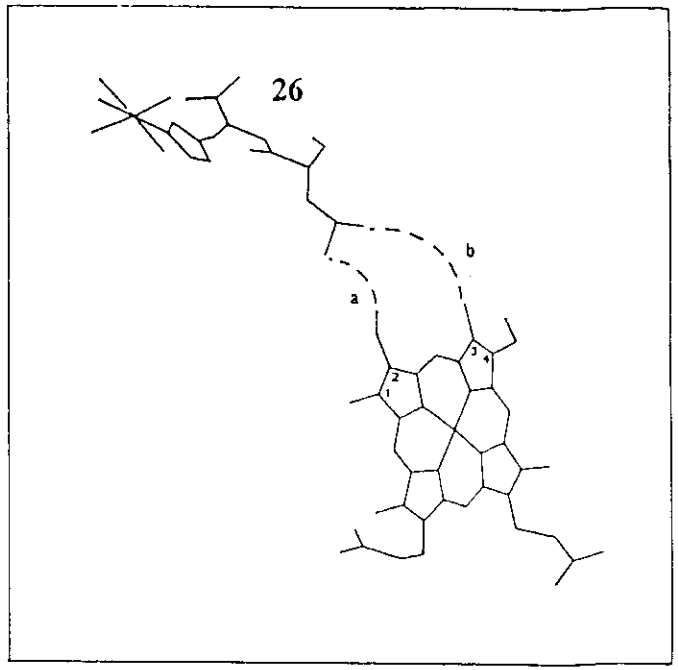

Figure 6 Best-pathway through-space jump from Leu25 to the heme in Ru(His26)-modified cytochrome Tb_5(*a*) and DPb_5 (*b*).

group, which is the terminus of the Leu25-to-heme through-space jump in the other two proteins (40, 41). A longer jump to the heme 3-methyl is predicted for Rua_5(His26)DPb_5, leading to a slower electron-transfer rate.

NATURE OF THE PATHWAYS Pathways from His26 to the heme in cytochrome b_5 are somewhat less sparse than in cytochrome *c*. When the His63-Fe coupling (2.04-Å bond length) is treated as a through-space interaction, pathways through the vinyl group dominate as described above. Two other classes of pathways can be identified. Pathways arising from through-space interactions between the heme and residues His63 and Phe58 form a second tier of paths with weaker coupling than those described above.

Reorganization Energies and Electronic Couplings

Based on the few systems in which a reliable number has been extracted, $\lambda = 1.2$ eV appears to be a reasonable value for Ru-ammine-modified cytochromes (74a). Perhaps because of a lack of data and limited precision in the derived parameters, λ has not been found to be particularly sensitive to D-A separation or to the site of modification. In fact, the simple Marcus

cross relation provides a reasonably good estimate of the reorganization energies in these reactions.

Unlike the reorganization energy, the electronic-coupling strengths in the Ru-modified cytochromes show a great deal of variability. Equation 15 expresses a simple distance dependence for T_{DA} that adequately describes electron transfer in model complexes with values of β between 0.8 and 1.2 $Å^{-1}$. This distance dependence, assuming a maximum electron-transfer rate of 10^{13} s^{-1} at close contact ($d = 3$ Å), is represented by the solid ($\beta = 1.0$ $Å^{-1}$) and dashed ($\beta = 0.8$, 1.2 $Å^{-1}$) lines in Figure 7. Estimates of maximum electron-transfer rates (i.e. the rate at $-\Delta G^{\circ} = \lambda$) for Ru-modified cytochromes (Table 3) are plotted as a function of D-A separation (λ was assumed to be 1.2 eV for the cytochrome b_5 derivatives). Clearly all of the maximum rates lie below the values predicted by Equation 15; there is no simple correlation. The obvious conclusion is that, for a given D-A separation, the electronic coupling in the Ru-modified proteins is

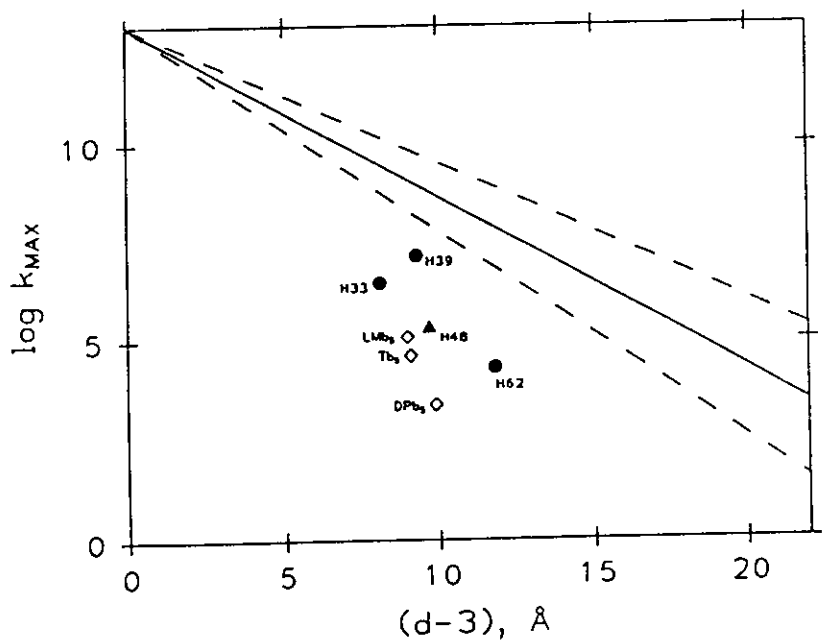

Figure 7 Plot of $\log k_{MAX}$ versus D-A distance (d) minus 3 Å (van der Waals contact) for Ru-modified proteins. Solid and dashed lines represent Equation 15 with $\beta = 0.8$, 1.0, and 1.2 $Å^{-1}$. Filled symbols indicate systems in which λ was estimated from a driving-force study. Open symbols indicate that an assumed value for λ (1.2 eV) was used to estimate k_{MAX}. ●, Cytochrome c; ▲, His48 derivative of Mb; ◇, His26 derivatives of cytochrome b_5.

Table 3 Maximum rates, D-A distances, coupling strengths, and effective bonds in pathways for Ru-modified proteins

	k_{max} (s^{-1})	d(Å)	T_{DA} (cm^{-1})	n_{eff} (bonds)
Ru(His39)cyt c[a]	1.4×10^{7}	12.3	0.24	14.0
Ru(His33)cyt c[b]	2.9×10^{6}	11.1	0.11	13.9
Ru(His62)cyt c[c]	2.0×10^{4}	14.8	0.01	20.6
Ru(His26)Tb_5[d]	4.1×10^{4}	12.1	0.01	19.0
Ru(His26)LMb_5[d]	1.2×10^{5}	12.0	0.02	18.7
Ru(His26)DPb_5[d]	2.4×10^{3}	12.9	0.003	20.3
Ru(His48)Mb[e]	2.1×10^{5}	12.7	0.03	22.6

[a] Reference 74.
[b] Reference 54.
[c] Reference 73.
[d] Reference 41.
[e] Reference 74a.

substantially weaker than that predicted by a simple exponential decay with distance.

Our pathway model predicts the failure of exponential-decay correlations based on edge-edge distances. It also predicts that maximum electron-transfer rates correlate with the effective number of bonds in the pathway. [Multiplying n_{eff} by a canonical value of 1.4 Å/bond gives a tunneling length (σl) that replaces d in rate-distance correlations.] Maximum electron-transfer rates in the Ru-modified cytochromes are plotted against σl in Figure 8. A linear least-square fit yields the solid line with a slope of 0.7 $Å^{-1}$. Though the data are limited, the intercept at one bond (i.e. 1.4 Å) corresponds to a maximum electron-transfer rate of 3.4×10^{12} s^{-1}, which is in reasonable agreement with data from covalently coupled D-A complexes (33, 37, 76).

RUTHENATED MYOGLOBIN

His48 Derivatives

Myoglobin (Mb) is an oxygen-storage protein with 153 amino acids and a heme prosthetic group (1). Unlike cytochrome c, the heme is not covalently bound to the protein in Mb. This feature greatly facilitates metal substitution and has enabled the preparation of Ru(His48) proteins with six different metalloporphyrin active sites.

For cytochrome c, the evidence indicated that the reorganization energy for the electron-transfer reactions of the Zn-substituted protein would be nearly the same as that of the native-Fe protein. This, however, is not

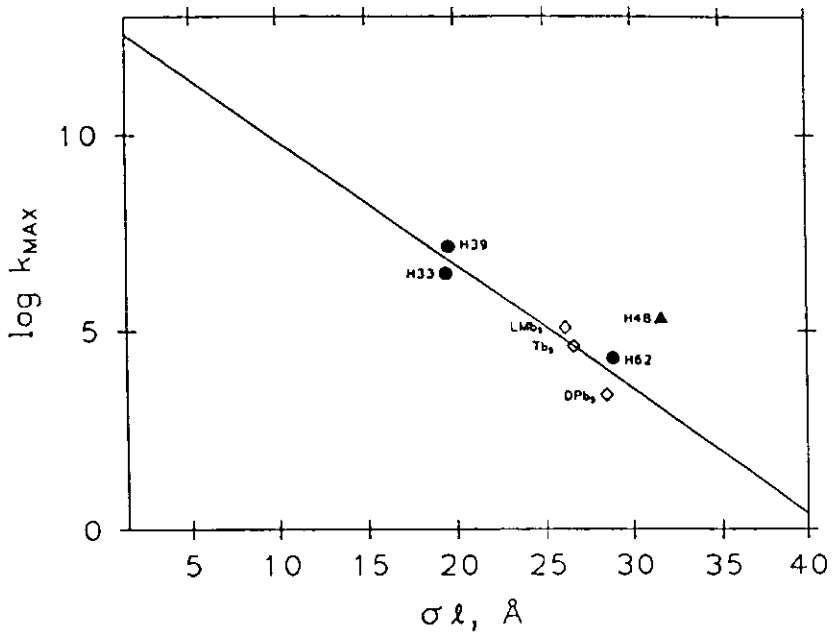

Figure 8 Plot of $\log k_{MAX}$ versus the tunneling length, σl ($= n_{eff} \times 1.4$ Å/bond), in the physical pathway between donor and acceptor for three Ru-modified derivatives of cytochrome *c* (●), three His26 derivatives of cytochrome b_5 (◇), and one Mb derivative (▲). The solid line is a linear least-square fit to the three cytochrome *c* points.

likely to be true in myoglobin: Fe(II)-Mb is a five-coordinate low-spin complex that, upon one-electron oxidation, binds a water molecule to form a six-coordinate species (1). This change in coordination number should be reflected in a greater reorganization energy in native Fe Mb, or even by electron-transfer rates limited by ligand binding or dissociation. The electron-transfer reactions of Ru-modified, metal-substituted Mb, however, are not accompanied by changes in metal coordination, and a single set of electron-transfer parameters should adequately describe these reactions. The rates of 18 different electron-transfer reactions in Ru(His48) Mb have been reported (Table 4) (2, 22, 24, 44, 45, 74a), spanning nearly 0.8 eV in driving force. Fitting the photoinduced and thermal recombination rates to a classical expression for *FC* yields $\lambda = 1.26$ eV and $T_{DA} = 0.03$ cm^{-1} (74a). The D-A separation in Ru(His48)Mb (12.7 Å) is quite similar to the distances in His33 and His39 derivatives of cytochrome *c* and does not readily explain the smaller value of T_{DA}. The best pathway in Ru(His48)Mb, however, is comprised of 22.6 effective bonds (eight more than found in the His33 and His39 pathways).

Table 4 Electron-transfer rates in Ru(His48)-modified myoglobin

Electron transfer	$-\Delta G^{\circ}$ (eV)	k_{ET} (s^{-1})
$H_2P^* \rightarrow Ru^{II}_5(His)^{[a]}$	0.39(±2)	$7.6(8) \times 10^{2}$
$Ru^{II}_4(isn)(His)^{2+} \rightarrow ZnP^{+[b]}$	0.61(±2)	$1.4(5) \times 10^{4}$
$PdP^* \rightarrow Ru^{II}_5(His)^{[c]}$	0.64(±2)	$9.1(9) \times 10^{3}$
$Ru^{II}_4(py)(His)^{2+} \rightarrow ZnP^{+[b]}$	0.69(±2)	$2.0(5) \times 10^{4}$
$CdP^* \rightarrow Ru^{II}_5(His)^{[a,d]}$	0.79(±2)	$4.5(5) \times 10^{4}$
$MgP^* \rightarrow Ru^{II}_5(His)^{[a,d]}$	0.81(±2)	$9.5(9) \times 10^{4}$
$ZnP^* \rightarrow Ru^{II}_5(His)^{[b]}$	0.82(±2)	$7.0(7) \times 10^{4}$
$PdP^* \rightarrow Ru^{II}_4(py)(His)^{[c]}$	0.91(±2)	$9.0(9) \times 10^{4}$
$Ru^{II}_5(His)^{2+} \rightarrow MgP^{+[d]}$	0.91(±2)	$4.9(5) \times 10^{4}$
$Ru^{II}_5(His)^{2+} \rightarrow CdP^{+[d]}$	0.92(±2)	$2.1(2) \times 10^{5}$
$Ru^{II}_5(His)^{2+} \rightarrow ZnP^{+[b]}$	0.96(±2)	$1.5(5) \times 10^{5}$
$ZnP^* \rightarrow Ru^{II}_4(py)(His)^{[b]}$	1.09(±2)	$2.0(2) \times 10^{5}$
$ZnP^* \rightarrow Ru^{II}_4(isn)(His)^{[b]}$	1.17(±2)	$2.9(3) \times 10^{5}$
$Ru^{II}_5(His)^{2+} \rightarrow Fe(II)(CN\text{-}Br)^{[e]}$	0.09(±2)	2.0(5)
$Fe(II)(CN\text{-}Br) \rightarrow Ru^{III}_4(isn)(His)^{[e]}$	0.26(±2)	5.5(5)
$Fe(II) \rightarrow Ru^{III}_5(His)^{[f]}$	0.02(±2)	$4.0(5) \times 10^{-2}$
$Fe(II) \rightarrow Ru^{III}_4(py)(His)^{[g]}$	0.28(±2)	2.5(5)
$Fe(II) \rightarrow Ru^{III}_4(isn)(His)^{[g]}$	0.35(±2)	3.0(4)

[a] Reference 22.
[b] References 44, 74a.
[c] Reference 45.
[d] Reference 74a.
[e] Reference 79.
[f] Reference 24.
[g] Reference 49.

Cyanogen-bromide modification of His64 in the distal heme pocket of myoglobin inhibits coordination of a water ligand to the ferric heme (43, 56, 69). Therefore the reorganization energy for electron transfer in cyanogen-bromide-treated Ru(His48)-Fe-Mb will probably be nearly the same as that of the metal-substituted myoglobins. Fitting the two electron-transfer rates measured for this system (Table 4) to Equation 2, with λ equal to 1.26 eV, yields an electronic-coupling matrix element of 0.01 cm^{-1} (79). As in the case of Ru-modified cytochrome *c*, the apparent coupling strength in Ru-ammine–iron-heme reactions is somewhat smaller than that found for reactions involving Ru-ammines and metal-substituted porphyrins.

Three electron-transfer rates have been measured with Ru-ammines bound to His48 of native Fe myoglobin (Table 4) (24, 49). The reorganization energy for these reactions can be estimated by assuming that the coupling strength is the same as that found in the cyanogen bromide–treated systems (0.01 cm^{-1}) and by optimizing λ. The data suggest $\lambda = 1.48$

eV (74a), a 0.2-eV increase over the value found in systems that have no change in coordination number.

Nature of the Pathways

The pathways in cytochrome *c* are rather sparse and fairly independent compared to pathways in His48 Mb (Figure 4). This Mb derivative has two or three families of pathways, one connected to the heme by a hydrogen bond to Arg45, one connected through space to Phe43, and one connected through space to Lys42. In contrast to cytochrome *c*, loops interconnect these paths (by hydrogen-bond and through-space interactions) throughout the protein. The limitations of the single pathway approximation depend on the number of loops in the intervening medium, and it will be interesting to see (theoretically as well as experimentally) how well single-pathway models work for proteins of varied structural motifs.

Figure 8 also plots the maximum electron transfer rate for His48-modified Mb (n_{eff} = 22.6 bonds) (74a). This Mb point lies substantially above the line based on the cytochrome *c* and b_5 data, and clearly indicates a problem with the pathway model. In the simple form of this model, a single route is assumed to dominate the D-A coupling. The pathway-searching algorithm tends to support this assumption in the cytochromes, where single coupling paths stand out. In Mb, however, the pathway-searching algorithm identifies many nearly equivalent pathways: the one used for the point in Figure 8 represents the best route, but there are several close competitors. The problem is again the tunneling distance: with many nearly equivalent paths contributing to D-A coupling, n_{eff} will be substantially below 22.6 bonds for His48 Mb. Efforts are being made to refine the pathway model to accommodate multiple paths. If enough paths contribute to the overall electronic coupling in a given protein, the composition of any one path becomes relatively unimportant and tunneling lengths should closely parallel edge-edge distances.

CONCLUDING REMARKS

In addition to the utility of the pathway-mapping method in examining couplings between pairs of points in proteins, its simplicity allows the generation of global coupling maps from all atoms in a protein to the redox center. Such maps reveal important characteristic effects of primary, secondary, tertiary, and quaternary folded structure on the nature of the coupling to a specific patch of the protein. Regions anomalously strongly or weakly coupled to the redox center, given their distances, are easily identified (3), and evidence of these anomalous regions should appear in the experimental data. The simple pathway model appears to work relatively well for the cytochromes, which have few pathways. The His48 Mb data are not entirely consistent with the single-pathway analysis discussed here. Differences can arise from inadequacy of the single-path approximation, uncertainties in fitting of the experimental data, and inadequacies of using a simple classical expression for *FC*.

Our pathway technique is now being used to study other biological systems (19, 21, 29, 31, 32, 39, 57). New theoretical strategies are being implemented to further our understanding of tunneling pathways so that greater molecular detail can be included in the treatment of very large systems (see 66 for a description of the methods used). The long-term goal of this work is to obtain compact symbolic representations for proteins that include all the relevant pathways in the protein.

ACKNOWLEDGMENTS

Work in San Diego was funded by the National Science Foundation (Grant No. DMB-9018768) and a research contract from the Jet Propulsion Laboratory, supported by the Department of Energy's Catalysis/Biocatalysis Program. This work was performed in part at the Jet Propulsion Laboratory, California Institute of Technology, and was sponsored by the Department of Energy's Catalysis/Biocatalysis Program (Advanced Industrial Concepts Division), through an agreement with the National Aeronautics and Space Administration. Experimental work at the Beckman Institute was supported by the National Science Foundation and the National Institutes of Health.

Literature Cited

1. Antonini, E., Brunori, M. 1971. *Hemoglobin and Myoglobin in Their Reactions with Ligands*. Amsterdam: North Holland
2. Axup, A. W., Albin, M., Mayo, S. L., Crutchley, R. J., Gray, H. B. 1988. *J. Am. Chem. Soc.* 110: 435
3. Beratan, D. N., Betts, J. N., Onuchic, J. N. 1991. *Science* 252: 1285
4. Beratan, D. N., Hopfield, J. J. 1984. *J. Am. Chem. Soc.* 106: 1584
5. Beratan, D. N., Hopfield, J. J. 1984. *J. Chem. Phys.* 81: 5753
6. Beratan, D. N., Onuchic, J. N. 1989. *Photosynth. Res.* 22: 173
7. Beratan, D. N., Onuchic, J. N. 1991. *Adv. Chem. Ser.* 228: 71
8. Beratan, D. N., Onuchic, J. N., Betts, J. N., Bowler, B. E., Gray, H. B. 1990. *J. Am. Chem. Soc.* 112: 7915
9. Beratan, D. N., Onuchic, J. N., Gray, H. B. 1991. See Ref. 72, p. 97
10. Beratan, D. N., Onuchic, J. N., Hopfield, J. J. 1985. *J. Chem. Phys.* 83: 5325
11. Beratan, D. N., Onuchic, J. N., Hopfield, J. J. 1987. *J. Chem. Phys.* 86: 4488
12. Bialek, W., Bruno, W. J., Joseph, J., Onuchic, J. N. 1989. *Photosynth. Res.* 22: 15
13. Bowler, B. E., Meade, T. J., Mayo, S. L., Richards, J. H., Gray, H. B. 1989. *J. Am. Chem. Soc.* 111: 8757
14. Broo, S., Larsson, S. 1989. *J. Quant. Chem. Quant. Biol. Symp.* 16: 185
15. Brown, G. M., Sutin, N. 1979. *J. Am. Chem. Soc.* 101: 883
16. Brunschwig, B. S., Ehrenson, S., Sutin, N. 1986. *J. Phys. Chem.* 90: 3657
17. Buckley, F., Harary, F. 1990. *Distance in Graphs*. New York: Addison-Wesley

18. Caldeira, A. O., Leggett, A. J. 1983. *Ann. Phys.* 149: 374
19. Christensen, H. E. M., Conrad, L. S., Ulstrup, J., Mikkelsen, K. V. 1991. See Ref. 72, p. 57
20. Churg, A. K., Weiss, R. M., Warshel, A., Takano, T. 1983. *J. Phys. Chem.* 87: 1683
21. Conrad, D. W., Scott, R. A. 1989. *J. Am. Chem. Soc.* 111: 3461
22. Cowan, J. A., Upmacis, R. K., Beratan, D. N., Onuchic, J. N., Gray, H. B. 1988. *Ann. N.Y. Acad. Sci.* 550: 68
23. Cramer, W. A., Knaff, D. B. 1990. *Energy Transduction in Biological Membranes.* New York: Springer-Verlag
24. Crutchley, R. J., Ellis, W. R., Gray, H. B. 1985. *J. Am. Chem. Soc.* 107: 5002
25. da Gama, A. A. S. 1985. *Theor. Chim. Acta* 68: 159
26. da Gama, A. A. S. 1990. *J. Theor. Biol.* 142: 251
27. Davydov, A. S. 1987. *Phys. Status Solidi B* 90: 457
28. DeVault, D. 1984. *Quantum Mechanical Tunneling in Biological Systems.* New York: Cambridge Univ. Press. 2nd ed.
29. Durham, B., Pan, L. P., Long, J. E., Millett, F. 1989. *Biochemistry* 28: 8659
30. Elias, H., Chou, M. H., Winkler, J. R. 1988. *J. Am. Chem. Soc.* 110: 429
31. Farver, O., Pecht, I. 1989. *FEBS Lett.* 244: 379
32. Feher, G., Allen, J. P., Okamura, M. Y., Rees, D. C. 1989. *Nature* 339: 111
33. Fox, L. S., Kozik, M., Winkler, J. R., Gray, H. B. 1990. *Science* 247: 1069
34. Garg, A., Onuchic, J. N., Ambegaokar, V. 1985. *J. Chem. Phys.* 83: 4491
35. Goldman, C. 1991. *Phys. Rev. A* 43: 4500
36. Gray, H. B., Malmström, B. G. 1989. *Biochemistry* 28: 7499
37. Holten, D., Hoganson, C., Windsor, M. W., Schenck, C. C., Parson, W. W., et al. 1980. *Biochim. Biophys. Acta* 592: 461
38. Hopfield, J. J. 1974. *Proc. Natl. Acad. Sci. USA* 71: 3640
39. Jackman, M. P., McGinnis, J., Powls, R., Salmon, G. A., Sykes, A. G. 1988. *J. Am. Chem. Soc.* 110: 5880
40. Jacobs, B. A. 1991. *Preparation, characterization, and intramolecular electron transfer in pentaammineruthenium-modified derivatives of cytochrome* b_5 *and azurin.* PhD Thesis. Calif. Inst. Technol., Pasadena, Calif.
41. Jacobs, B. A., Mauk, M. R., Funk, W. D., MacGillivray, R. T. A., Mauk, A. G., Gray, H. B. 1991. *J. Am. Chem. Soc.* 113: 4390
42. Jortner, J. 1980. *Biochim. Biophys. Acta* 594: 139
43. Kamiya, N., Shiro, Y., Iwata, T., Iizuka, T., Iwasaki, H. 1991. *J. Am. Chem. Soc.* 113: 1826
44. Karas, J. L. 1989. *Long-range electron transfer in ruthenium-labelled myoglobin.* PhD Thesis. Calif. Inst. Technol., Pasadena, Calif.
45. Karas, J. L., Lieber, C. M., Gray, H. B. 1988. *J. Am. Chem. Soc.* 110: 599
46. Kuki, A., Wolynes, P. G. 1987. *Science* 236: 1647
47. Larsson, S. 1981. *J. Am. Chem. Soc.* 103: 4034
48. Larsson, S. 1983. *J. Chem. Soc. Faraday Trans.* 279: 1375
49. Lieber, C. M., Karas, J. L., Gray, H. B. 1987. *J. Am. Chem. Soc.* 109: 3779
50. Lin, S. H. 1989. *J. Chem. Phys.* 90: 7103
51. Marcus, R. A., Sutin, N. 1985. *Biochim. Biophys. Acta* 811: 265
52. Magarshak, Y., Malinsky, J., Joran, A. D. 1991. *J. Chem. Phys.* 95: 418
53. McConnell, H. M. 1961. *J. Chem. Phys.* 35: 508
54. Meade, T. J., Gray, H. B., Winkler, J. R. 1989. *J. Am. Chem. Soc.* 111: 4353
55. Mikkelsen, K. V., Ratner, M. A. 1988. *Chem. Rev.* 87: 113
56. Morishima, I., Shiro, J., Wakino, T. 1985. *J. Am. Chem. Soc.* 107: 1063
57. Natan, M. J., Baxter, W. W., Kuila, D., Gingrich, D. J., Martin, G. S., Hoffman, B. M. 1991. *Adv. Chem. Ser.* 228: 201
58. Newton, M. D. 1988. *J. Phys. Chem.* 92: 3049
59. Newton, M. D. 1991. *Chem. Rev.* 91: 767
60. Newton, M. D., Sutin, N. 1984. *Annu. Rev. Phys. Chem.* 35: 437
61. Nocera, D. G., Winkler, J. R., Yocom, K. M., Bordignon, E., Gray, H. B. 1984. *J. Am. Chem. Soc.* 106: 5145
62. Onuchic, J. N. 1987. *J. Chem. Phys.* 86: 3925
63. Onuchic, J. N., Beratan, D. N. 1987. *J. Am. Chem. Soc.* 109: 6771
64. Onuchic, J. N., Beratan, D. N. 1990. *J. Chem. Phys.* 92: 722
65. Onuchic, J. N., Beratan, D. N., Hopfield, J. J. 1986. *J. Phys. Chem.* 90: 3707
66. Onuchic, J. N., de Andrade, P. C. P., Beratan, D. N. 1991. *J. Chem. Phys.* 92: 1131
67. Onuchic, J. N., Wolynes, P. G. 1988. *J. Phys. Chem.* 92: 6495
67a. Ratner, M. A. 1990. *J. Phys. Chem.* 94: 4877
68. Selman, M. A. 1989. *Preparation and characterization and intramolecular electron transfer in a pentaammineruthenium derivative of* Candida krusei *cytochrome c.* PhD Thesis. Calif. Inst. Technol., Pasadena, Calif.
69. Shiro, Y., Morishima, I. 1984. *Biochemistry* 23: 4879
70. Siddarth, P., Marcus, R. A. 1990. *J. Phys. Chem.* 94: 2985
71. Siddarth, P., Marcus, R. A. 1990. *J. Phys. Chem.* 94: 8430
72. Sigel, H., Sigel, A., eds. 1991. *Metal Ions in Biological Systems*, Vol. 27. New York: Marcel Dekker
73. Therien, M. J., Bowler, B. E., Selman, M. A., Gray, H. B., Chang, I.-J., Winkler, J. R. 1991. *Adv. Chem. Ser.* 228: 191
74. Therien, M. J., Selman, M. A., Gray, H. B., Chang, I.-J., Winkler, J. R. 1990. *J. Am. Chem. Soc.* 112: 2420
74a. Winkler, J. R., Gray, H. B. 1992. *Chem. Rev.* In press
75. Winkler, J. R., Nocera, D. G., Yocom, K. M., Bordignon, E., Gray, H. B. 1982. *J. Am. Chem. Soc.* 104: 5798
76. Wasielewski, M. R., Niemczyk, M. P., Svec, W. A., Pewitt, E. B. 1985. *J. Am. Chem. Soc.* 107: 5562
77. Yocom, K. M. 1981. *The synthesis and characterization of inorganic redox reagent-modified cytochrome c.* PhD Thesis. Calif. Inst. Technol., Pasadena, Calif.
78. Yocom, K. M., Shelton, J. B., Shelton, J. R., Schroeder, W. E., Worosila, G., et al. 1982. *Proc. Natl. Acad. Sci. USA* 79: 7052
79. Zewert, T. E. 1990. *Electron transfer in chemically and genetically modified myoglobins.* PhD Thesis. Calif. Inst. Technol., Pasadena, Calif.

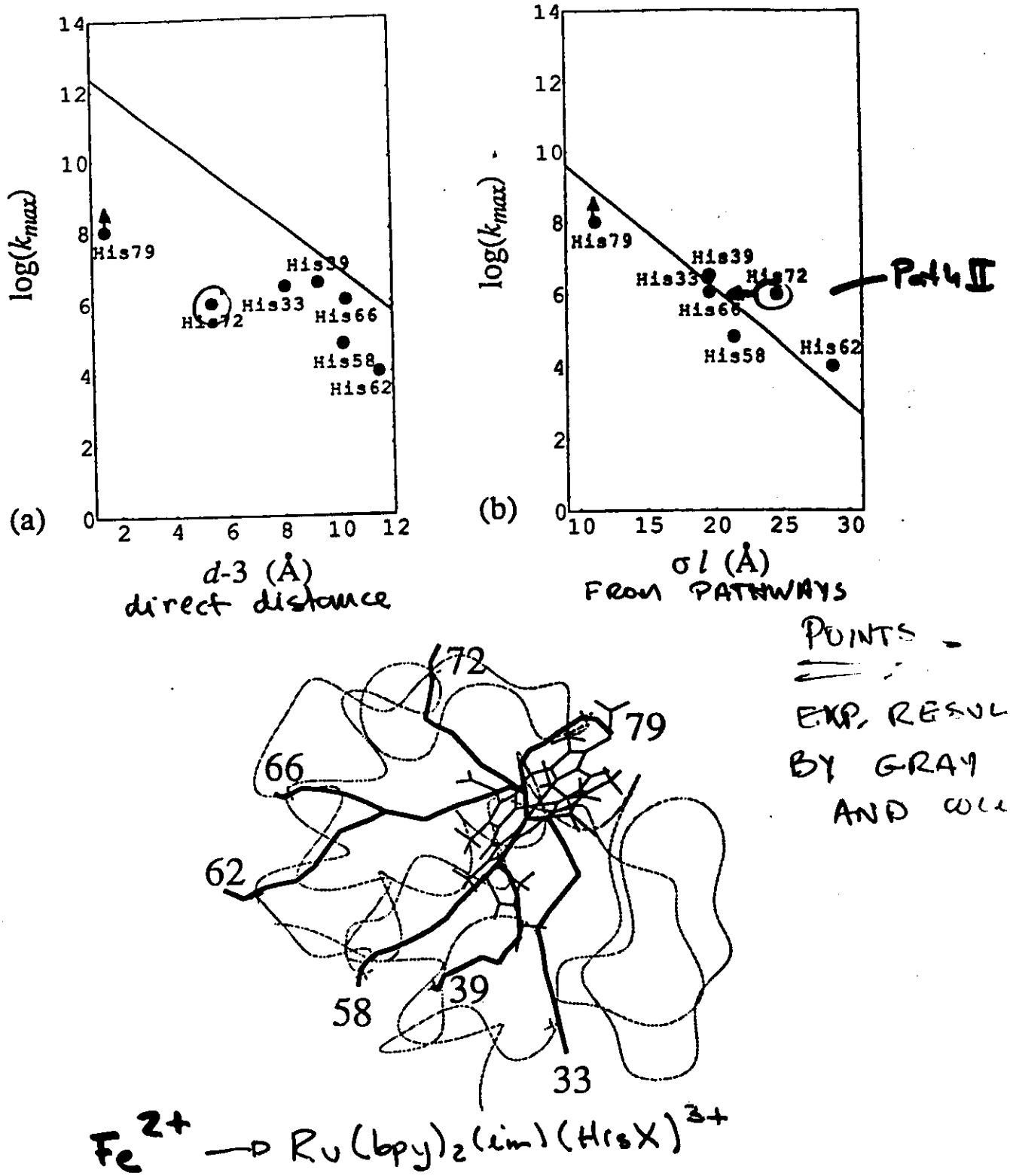

Figure 4 – ET rates in Ru modified cytochrome *c*. Electron transfer rates from Fe^{2+} to $Ru(bpy)_2(im)(HisX)^{3+}$ are presented. (a) Correlations of activationless ET rates (k_{max}) with the direct distance (d) between *D–A*. The solid line shows the rates predicted by Dutton, $10^{13}\exp[-1.4(d-3)]$ sec^{-1}. (b) Correlation of k_{max} with the effective covalent distance (σl). The agreement between the experimental data and *Pathways* (solid line) is excellent.

Donor-Acceptor Electronic Coupling in Ruthenium-Modified Heme Proteins

Danilo R. Casimiro,[§] David N. Beratan,[†] José Nelson Onuchic,[‡] Jay R. Winkler,[§] and Harry B. Gray[§]

[†] Department of Chemistry, University of Pittsburgh, Pittsburgh, PA 15260

[‡] Department of Physics, University of California, San Diego, La Jolla, CA 92093

[§] Beckman Institute, California Institute of Technology, Pasadena, CA 91125

Abstract. The rates of electron transfer (ET) in six ruthenium-modified cytochrome *c* derivatives have been analyzed in terms of four theoretical models describing donor-acceptor electronic coupling. The simplest model, which treats the protein as a homogeneous medium, fails to describe the variations in ET rates with changes in donor-acceptor separation. The three other models explicitly account for the inhomogeneity of the polypeptide matrix and are more successful in describing the electronic couplings. Calculations of relative coupling strengths give results within an order or magnitude of experimentally determined values for cytochrome *c*. The homogenous-medium model is more successful in describing ET in Ru-modified myoglobin, and two of the inhomogeneous-medium models suggest that multiple pathways are important in mediating the electronic coupling.

ACS Books: Mechanistic Bioinorganic Chemistry
H. Thorp and V. Pecoraro, eds., ACS Press
Washington D.C., in press

Many bioenergetic and biosynthetic processes involve electron transfer (ET) steps in which an electron tunnels several angstroms from donor to acceptor through protein (1). The problem of understanding the detailed mechanisms of these processes is being addressed experimentally through studies of ET in synthetic model complexes (2-4), in chemically modified metalloproteins (5), and in protein complexes (6-8). Theoretical efforts are aimed at describing the electronic coupling between distant redox sites (9-21) and at clarifying the importance of protein conformational dynamics in regulating ET (22). A particular emphasis of our work is to identify the role of the protein matrix in mediating biological electron transfer.

The weak electronic coupling between distant donor and acceptor sites leads to long-range ET rates (k_{ET}) that are well-described by a nonadiabatic formulation (23):

$$k_{ET} = \frac{2\pi}{\hbar} |T_{DA}|^2 (F.C.) \tag{1}$$

The rate is proportional to an electronic coupling factor, $|T_{DA}|^2$, and a Franck-Condon factor ($F.C.$) arising from nuclear motion coupled to the ET process. The $F.C.$ factor describes the tradeoff between reaction free energy and the nuclear reorganization energy. At the optimum driving force, $F.C.$ is unity and rates reach a maximum value (k_{max}), limited by $|T_{DA}|^2$. The simplest description of T_{DA} treats the medium between donor and acceptor as a one-dimensional square tunneling barrier (1DSB). As such, the rate is predicted to drop exponentially with distance (24,25):

$$k_{ET}^{1DSB} = \frac{2\pi}{\hbar} |T_{DA}(R_0)|^2 \exp[-\beta(R-R_0)](F.C.) \tag{2}$$

Accounting for the role of protein-mediated coupling in the 1DSB models amounts to assigning a barrier height for electron tunneling. Early estimates of the electronic coupling decay constants by Hopfield (β = 1.4 Å^{-1}) (24) and Jortner (β = 2.6 Å^{-1}) (25) stimulated numerous experiments on small molecules and proteins of varied bridge structure. Both proteins and hydrocarbon bridges of known structure were used to link donors and acceptors. Homologous series of organic compounds were reported that displayed different β values. Improved theoretical analysis showed that much of this diversity could arise from bridge orbital-energy and symmetry effects. Dutton and coworkers have suggested that the uniform 1DSB model for electron tunneling, with a single exponential decay constant (eq 2), qualitatively describes a broad range of natural and synthetic ET systems (26,27). The value of β derived for biological ET systems was 1.4 Å^{-1}. This treatment provides a reliable zero-order estimate of coupling strengths for many protein ET systems over a wide range of donor-acceptor separations. There are, however, discrepancies that may be due to specific structural aspects of the proteins involved.

A 1DSB is a crude approximation to a polypeptide matrix. A more sophisticated model can be developed by decomposing the protein medium between two redox sites into smaller subunits (28-31). The coupling between the termini in a bridge comprised of identical repeating units drops by a simple multiplicative factor (ϵ) as the chain is lengthened. This value of ϵ depends on the energy of the tunneling electron as well as on the composition of the repeat unit in the bridge. For simplicity, the decay can be divided into components associated with each bonded and nonbonded contact within the repeat unit.

The convenient and practical "decay per unit" strategy can be readily extended to

aperiodic protein structures by differentiating among the many types of interactions present in a protein structure. Tunneling is much more efficient (decays more slowly) through bonded orbitals than through-space, because the potential barrier is effectively lower. In proteins, the covalently bonded path between donor and acceptor can be extremely long compared to the direct through-space distance. As a first approximation, we distinguish only between covalent bonds, hydrogen bonds, and nonbonded contacts. If a single pathway dominates the matrix element (9):

$$T_{DA} \propto \prod_i \epsilon_c(i) \prod_j \epsilon_H(j) \prod_k \epsilon_S(k) \tag{3}$$

Just as the ϵ's are highly "renormalized" parameters in the periodic chain calculation, these decay factors are also renormalized for proteins. The values of the parameters take into account, in an average way, high order contributions to the coupling, a distribution in bond energies and interactions, *etc.* Any combination of covalent, hydrogen-bonded, and through-space contacts between the donor and acceptor sites defines a specific physical tunneling pathway.

We estimate relative tunneling matrix elements by finding the single physical pathway that maximizes the product in eq 3 using the parameters (9):

$$\epsilon_C = const. \approx 0.6 \tag{4a}$$

$$\epsilon_H = \epsilon_C^2 \exp[-1.7(R-2R_C)] \tag{4b}$$

$$\epsilon_S = \sigma_S \epsilon_C \exp[-1.7(R-R_C)] \approx 0.5 \epsilon_C \exp[-1.7(R-R_C)] \quad (4c)$$

The constant chosen for ϵ_C is usually 0.6 and for σ_S (the average through-space orientation factor) is 0.5. These parameters are based on experiments, where available, and on theory where experiments are preliminary or sparse. Most importantly, the nature of the dominant paths does not change drastically as the parameters are varied over a physically reasonable range. The most critical parameter of the model is the value of ϵ_C relative to the exponential decay of through-space interactions.

Using the decay factors in eqs 3 and 4, one can search for the lowest order contributions to T_{DA}. In this way, a macromolecule electronic structure problem is reduced to the relatively simple task of finding the minimum distance in a graph. The minimum-distance problem is well known and can be solved in a reasonable amount of time. Thus, a given protein structure defines the connectivity and decay factors between neighboring sites according to the prescription in eq 3, and the optimum coupling pathways between any two points are readily calculated.

The 1DSB model for protein ET predicts that ln k_{ET} should scale linearly with distance. In the tunneling pathway (TP) model, rates should scale with the product of decay factors in eq 3. Thus, if pathways between donor and acceptor consist of a small number of strong links (covalent or hydrogen-bonded connections), the couplings and maximum rates will be large. If, however, a donor-acceptor pair has circuitous bonded pathways (*i.e.*, a large number of covalent or hydrogen-bonded links) or weak direct paths (*i.e.*, long or numerous through-space contacts), the maximum rate will be anomalously slow. These qualitative expectations can be quantified

by calculating the effective tunneling pathway length, $\sigma\ell$ (= [ln $\Pi_i\epsilon(i)$/ln ϵ_C]R_C]). ET rates should drop exponentially with the tunneling pathway length rather than the physical distance between donor and acceptor. The value of $\epsilon_C = 0.6$ implies an exponential decay constant of $\beta' = 0.73$ Å^{-1}.

A hybrid approach to the electronic coupling problem in proteins has been introduced by Siddarth and Marcus (10-12). In this method, a protein-searching algorithm is combined with extended Hückel calculations on a subset of amino acids in the protein. In the first stage of the calculation, an artificial-intelligence (AI) searching routine is employed to identify the amino-acid residues that contribute significantly to donor-acceptor coupling. As with the TP model, a search of the protein structure for important residues reduces the complexity of the electronic structure problem. These residues are then used as a basis in an extended Hückel calculation of the electronic coupling matrix element T_{DA}. The method is not expected to produce highly accurate *absolute* values of T_{DA}, but is expected to describe *relative* values of this matrix element.

Cytochrome *c*

Our approach to studying the effects of the inhomogeneous protein medium on ET rates is to probe different sections of a single protein at many predefined distances and intervening structures by modifying surface sites with redox-active probes (5). We have completed measurements of intramolecular electron transfer on six different ruthenium derivatives of wild-type and mutant cytochromes *c* (32-35). Each derivative contains a histidine residue that is covalently modified with a bis(2,2′-bipyridine)imidazoleruthenium complex. The histidine

residues are either naturally occurring (His33 of horse cytochrome *c*, His39 of *Candida krusei* cytochrome *c*), introduced semisynthetically (His72 of horse cytochrome *c*), or genetically engineered (His58, His62, and His66 of *Saccharomyces cerevisiae iso*-1-cytochrome *c*).

The rates of intramolecular $Fe^{2+} \rightarrow Ru^{3+}$ electron transfer were measured using a flash-quench technique (32); the results are listed in Table 1 along with other pertinent ET parameters. Measured ET rates span two orders of magnitude and a 6-Å range of edge-edge donor-acceptor separations. Maximum ET rates, k_{max}, have been estimated using a classical expression for *F.C.* (λ = 0.8 eV) (23).

The 1DSB model (using Dutton's parameters, β = 1.4 Å^{-1} and $k_{max}(R = 3 \text{ Å} = R_o) = 10^{13}$ s^{-1}) consistently predicts ET rates faster than are observed, and k_{max} is not strongly correlated with *R* (Figure 1) (33-35). The systematic deviations could be corrected by choosing a more appropriate distance measure (*e.g.*, metal-to-metal rather than edge-to-edge) or, equivalently, a smaller value of k_{max} at close contact. The scatter, however, reflects a weakness in the 1DSB model, most likely its failure to account for the inhomogeneous nature of the intervening medium.

Explicit inclusion of the protein structural details, even at the relatively basic level of the TP model, leads to a noticeable improvement over the 1DSB model. A plot of *log* k_{max} vs. $\sigma\ell$ appears in Figure 2. The solid line is the the best fit to the data with β' constrained to a value of 0.73 Å^{-1}. It is clear that the ET rates correlate much better with $\sigma\ell$ than with R, indicating that the structural details of the intervening protein medium are important in determining donor-acceptor coupling strengths.

The results of the TP calculation also can be represented as a plot of *log* k_{max}*(exptl) vs.*

log k_{max}*(calcd)* (Figure 3). The TP model does not calculate absolute coupling strengths; values of k_{max}*(calcd)* were obtained from the intercept of the line in Figure 2. The TP model does a very good job of describing k_{max} in four of the six ET rates for the Ru-modified cytochromes, and is within about one order of magnitude for the other two systems. Given that the TP model assumes only three types of interactions, the agreement is remarkable. The simplicity of the model may be responsible, in part, for some of the deviations apparent in Figures 2 and 3. The assumption that a single pathway dominates the coupling between redox sites may also contribute to the discrepancies.

Direct calculation of T_{DA} at the extended Hückel level (using amino acids identified in an AI search) provides a good correlation of k_{max}*(exptl)* with k_{max}*(calcd)*, although only four of the six modified cytochromes have been analyzed (11). Again, scaling of the calculated values is required to eliminate a systematic deviation from experimental values. It is interesting to compare the dominant pathways identified in the AI search to those found using the TP algorithm (Figure 4). Both models find the same link between His33 and the heme: direct coupling along the peptide from His33 to Pro30, then a H-bonded contact between the carboxyl oxygen of Pro30 and N(1) of the His18 imidazole. Substantially different pathways are found, however, for the His39, His62, and His72 derivatives. The discrepancies could be the result of the different criteria used in determining couplings between groups. The large differences in the His72 pathways are, nevertheless, surprising. No excursions through Thr78 are found in the TP searches, yet this residue is involved in the best pathway found in the AI search.

It is clear that the homogeneous barrier model for electronic couplings is not adequate for cytochrome *c* and a model that includes the explicit structure of the intervening medium is

needed to provide a semiquantitative description of the tunneling process. Simple 1DSB models capture the overall decay of coupling for a very large range of distances and rates and agree with pathway models in their average values of β, although different proteins are predicted to have different average β values (28). The 1DSB models do not, however, account for the observed data scatter arising from the three-dimensional structures of the cytochromes that have been examined. The TP model contains a sufficiently detailed description of the medium to account for the considerable rate differences in the Ru-labeled cytochromes *c* that are inconsistent with 1DSB models. The AI searches and extended Hückel calculations also provide good agreement with experiment. In both cases, the data indicate that the structure of the intervening protein is absolutely critical in determining the rates of biological ET reactions.

A point of special interest is that the electronic couplings for intramolecular ET reactions in His58 and His66 cytochromes *c* are not enhanced by aromatic residues (Trp59 and Tyr69) in the intervening media (35). The correlation of ET rates with $\sigma\ell$ does not preclude a coupling role for the π orbitals of the aromatic groups in the pathway, but it does indicate that, in the Ru-modified cytochromes that we have examined, they are no more efficient in mediating the coupling than is the σ-bonded framework. Hence, the presence of aromatic groups in the medium between redox sites does not necessarily result in faster ET than in a purely aliphatic medium (15-20,36-40).

Gruschus and Kuki have developed an inhomogeneous aperiodic lattice (IAL) model to calculate the charge resonance energy (T_{DA}) for long-range electron transfer in proteins (13,14). The IAL treatment depends upon very careful calibration of diagonal and off-diagonal energies for specific protein subunits. Armed with these subunit matrix elements, the donor-acceptor

charge resonance energy is calculated using the *entire* protein structure. The objective of the IAL approach is to produce accurate absolute values of T_{DA}. IAL calculations of charge resonance energies have been performed for three Ru-ammine derivatives (His33, His39, and His62) of Zn-substituted cytochrome *c* (13). The calculated values of T_{DA}^2 are all within an order of magnitude of the experimentally derived quantities. Quantum interference effects were found to be particularly important in determining the overall coupling strength. In addition, all atoms within a ~ 10-Å-wide cross section between the redox sites were found to make significant contributions to the superexchange matrix element.

It should be noted that when quantum interference effects become extremely important, the calculated value of T_{DA} can become hypersensitive to the parameterization. Since the hamiltonian models used in all of these methods are approximate, it is absolutely critical to determine how sensitive the predictions of various methods are to small changes in the parameterization, particularly when destructive interference plays a significant role.

Myoglobin

ET data obtained for ruthenium-modified zinc-substituted human myoglobins (Mb) are set out in Table 1 (41). The simple pathway search algorithm finds many paths that contribute significantly to the donor-acceptor electronic coupling in each of the modified myoglobins. As expected for a protein system in which there is a high density of paths, the rates correlate with direct donor-acceptor separation. Although the dominant tunneling pathway significantly underestimates the coupling strength in each Mb derivative, a simple sum of best pathways (neglecting interferences) gives reasonably good agreement (Figure 5) (41). Good agreement

with experiment is also obtained by employing the AI method (42); in general, more amino acids are used in the calculations than comprise the dominant TP route (Figure 6). It is encouraging, however, that *both* the TP and AI analyses suggest that multiple pathways are important in mediating the electronic coupling in myoglobin.

Acknowledgments

We thank A. Kuki and R. A. Marcus for preprints of references 13 and 42, respectively. Beckman Young Investigator (JNO) and NSF-NYI (DNB) awards are acknowledged. This research was supported by the National Science Foundation, the National Institutes of Health, the Department of Energy, and the Arnold and Mabel Beckman Foundation.

Literature Cited

(1) *Metal Ions in Biological Systems*; Sigel, H.; Sigel, A., Ed.; Dekker: New York, 1991; Vol. 27.

(2) Closs, G. L.; Miller, J. R. *Science* **1988**, *240*, 440-447.

(3) Jordan, K. D.; Paddon-Row, M. N. *Chem. Rev.* **1992**, *92*, 395-410.

(4) Wasielewski, M. R. *Chem. Rev.* **1992**, *92*, 435-461.

(5) Winkler, J. R.; Gray, H. B. *Chem. Rev.* **1992**, *92*, 369-379.

(6) McLendon, G.; Hake, R. *Chem. Rev.* **1992**, *92*, 481-490.

(7) McLendon, G.; Zhang, Q.; Wallin, S. A.; Miller, R. M.; Billstone, V.; Spears, K. G.; Hoffman, B. M. *J. Am. Chem. Soc.* **1993**, *115*, 3665-3669.

(8) Wallin, S. A.; Stemp, E. D. A.; Everest, A. M.; Nocek, J. M.; Netzel, T. L.; Hoffman, B. M. *J. Am. Chem. Soc.* **1991**, *113*, 1842-1844.

(9) Onuchic, J. N.; Beratan, D. N.; Winkler, J. R.; Gray, H. B. *Annu. Rev. Biophys. Biomol. Struct.* **1992**, *21*, 349-377.

(10) Siddarth, P.; Marcus, R. A. *J. Phys. Chem.* **1990**, *94*, 2985-2989.

(11) Siddarth, P.; Marcus, R. A. *J. Phys. Chem.* **1990**, *94*, 8430-8434.

(12) Siddarth, P.; Marcus, R. A. *J. Phys. Chem.* **1992**, *96*, 3213-3217.

(13) Gruschus, J. M.; Kuki, A. *J. Phys. Chem.* in press.

(14) Gruschus, J. M.; Kuki, A. *Chem. Phys. Lett.* **1992**, *192*, 205-212.

(15) Christensen, H. E. M.; Conrad, L. S.; Mikkelsen, K. V.; Nielsen, M. K.; Ulstrup, J. *Inorg. Chem.* **1990**, *29*, 2808-2816.

(16) Christensen, H. E. M.; Conrad, L. S.; Hammerstad-Pedersen, J. M.; Ulstrup, J. *FEBS*

Lett. **1992**, *296*, 141-144.

(17) Christensen, H. E. M.; Conrad, L. S.; Mikkelsen, K. V.; Ulstrup, J. *J. Phys. Chem.* **1992**, *96*, 4451-4454.

(18) Broo, A. *Chem. Phys.* **1993**, *169*, 135-150.

(19) Broo, A. *Chem. Phys.* **1993**, *169*, 152-163.

(20) Broo, A.; Larsson, S. *J. Phys. Chem.* **1991**, *95*, 4925-4928.

(21) Larsson, S.; Broo, A.; Kallebring, B.; Volosov, A. *Int. J. Quant. Chem.* **1988**, *S15*, 1-22.

(22) Northrup, S. H.; Boles, J. O.; Reynolds, J. C. L. *Science* **1988**, *241*, 67-70.

(23) Marcus, R. A.; Sutin, N. *Biochim. Biophys. Acta* **1985**, *811*, 265-322.

(24) Hopfield, J. J. *Proc. Natl. Acad. Sci. USA* **1974**, *71*, 3640-3644.

(25) Jortner, J. *J. Chem. Phys.* **1976**, *64*, 4860-4867.

(26) Moser, C. C.; Keske, J. M.; Warncke, K.; Farid, R. S.; Dutton, P. L. *Nature* **1992**, *355*, 796-802.

(27) Farid, R. S.; Moser, C. C.; Dutton, P. L. *Curr. Opin. Struct. Biol.* **1993**, *3*, 225-233.

(28) Beratan, D. N.; Betts, J. N.; Onuchic, J. N. *Science* **1991**, *252*, 1285-1288.

(29) Onuchic, J. N.; Andrade, P. C. P.; Beratan, D. N. *J. Chem. Phys.* **1991**, *95*, 1131-1138.

(30) Onuchic, J. N.; Beratan, D. N. *J. Chem. Phys.* **1990**, *92*, 722-733.

(31) Beratan, D. N.; Onuchic, J. N. *Photosynth. Res.* **1989**, *22*, 173-186.

(32) Chang, I.-J.; Gray, H. B.; Winkler, J. R. *J. Am. Chem. Soc.* **1991**, *113*, 7056-7057.

(33) Wuttke, D. S.; Bjerrum, M. J.; Winkler, J. R.; Gray, H. B. *Science* **1992**, *256*,

1007-1009.

(34) Wuttke, D. S.; Bjerrum, M. J.; Chang, I.-J.; Winkler, J. R.; Gray, H. B. *Biochim. Biophys. Acta* **1992**, *1101*, 168-170.

(35) Casimiro, D. R.; Richards, J. H.; Winkler, J. R.; Gray, H. B. *J. Phys. Chem.* submitted.

(36) Farver, O.; Pecht, I. *J. Am. Chem. Soc.* **1992**, *114*, 5764-5767.

(37) Farver, O.; Skov, L. K.; Pascher, T.; Karlsson, B. G.; Nordling, M.; Lundberg, L. G.; Vänngard, T.; Pecht, I. *Biochemistry* **1993**, in press.

(38) Govindaraju, K.; Christensen, H. E. M.; Lloyd, E.; Olsen, M.; Salmon, G. A.; Tomkinson, N. P.; Sykes, A. G. *Inorg. Chem.* **1993**, *32*, 40-46.

(39) Everest, A. M.; Wallin, S. A.; Stemp, E. D. A.; Nocek, J. M.; Mauk, A. G.; Hoffman, B. M. *J. Am. Chem. Soc.* **1991**, *113*, 4337-4338.

(40) Bowler, B. E.; Meade, T. J.; Mayo, S. L.; Richards, J. H.; Gray, H. B. *J. Am. Chem. Soc.* **1989**, *111*, 8757-8759.

(41) Casimiro, D. R.; Wong, L.-L.; Colón, J. L.; Zewert, T. E.; Richards, J. H.; Chang, I.-J.; Winkler, J. R.; Gray, H. B. *J. Am. Chem. Soc.* **1993**, *115*, 1485-1489.

(42) Siddarth, P.; Marcus, R. A. *J. Phys. Chem.* **1993**, in press.

Table I. ET Parameters for Ru(HisX)-modified Cytochromes *c* and Human Myoglobin.

X [a]	k_{ET}, s^{-1} ($-\Delta G°$, eV)	k_{max}, s^{-1}	H_{AB}, cm^{-1}	**d**, Å	$\sigma\ell$, Å
		Cytochrome *c* [b]			
39	3.2×10^6 (0.74)	3.3×10^6	1.1×10^{-1}	12.3	19.6
33	2.6×10^6 (0.74)	2.7×10^6	9.7×10^{-2}	11.1	19.5
66	1.0×10^6 (0.77)	1.1×10^6	6.0×10^{-2}	13.3	19.6
72	9.0×10^5 (0.74)	9.4×10^5	5.7×10^{-2}	8.4	24.6
58	5.2×10^4 (0.69)	6.0×10^4	1.4×10^{-2}	13.2	21.4
62	1.0×10^5 (0.74)	1.0×10^4	5.9×10^{-3}	14.5	28.8
		Human Myoglobin [c]			
70	1.6×10^7 (0.82)	7.2×10^7	5.6×10^{-1}	9.5	24.3
48	7.2×10^4 (0.82)	3.3×10^5	3.8×10^{-2}	12.7	37.5
	1.1×10^5 (0.96)				
83	4.0×10^2 (0.82)	1.8×10^3	2.8×10^{-3}	15.5	43.5
	7.3×10^2 (0.96)				

[a] Cytochrome *c* modified with $Ru(bpy)_2(im)(HisX)$. Human myoglobin modified with $Ru(NH_3)_5(HisX)$.

[b] Values of k_{ET} correspond to $Fe^{2+} \rightarrow Ru(bpy)_2(im)(HisX)^{3+}$ ET; k_{max} and H_{AB} estimated using $\lambda = 0.8$ eV.

[c] Values of k_{ET} correspond to $^*ZnP \rightarrow Ru(NH_3)_5(HisX)^{3+}$ (upper) and $Ru(NH_3)_5(HisX)^{2+} \rightarrow ZnP^+$ (lower) ET; k_{max} and H_{AB} estimated using $\lambda = 1.3$ eV.

Figure Captions

1. Variation of maximum ET rates with edge-edge donor-acceptor distance in $Ru(bpy)_2(im)(HisX)$-modified cytochrome *c* (X = 33, 39, 58, 62, 66, 72).

2. (*Upper*) Dominant tunneling pathways in $Ru(bpy)_2(im)(HisX)$-modified cytochrome *c* (X = 33, 39, 58, 62, 66, 72). (*Lower*) Variation of maximum ET rates with tunneling length ($\sigma\ell$).

3. Correlation of calculated and experimental values of k_{max} for ET in $Ru(bpy)_2(im)(HisX)$-modified cytochrome *c*. (▲) TP calculation; (●) AI calculation.

4. Comparison of dominant tunneling pathways (*left*) and residues identified in AI searches (*right*) of $Ru(bpy)_2(im)(HisX)$-modified cytochrome *c* (X = 33 (*A*), 39 (*B*), 62 (*C*), 72 (*D*)).

5. Correlation of calculated and experimental values of k_{max} for ET in $Ru(NH_3)_5(HisX)$-modified human myoglobin. (▲) Multiple-path TP calculation; (●) AI calculation.

6. Comparison of dominant tunneling pathways (*left*) and residues identified in AI searches (*right*) of $Ru(NH_3)_5(HisX)$-modified Zn-substituted Mb (X = 70 (*A*), 48 (*B*), 83 (*C*)).

Figure 1

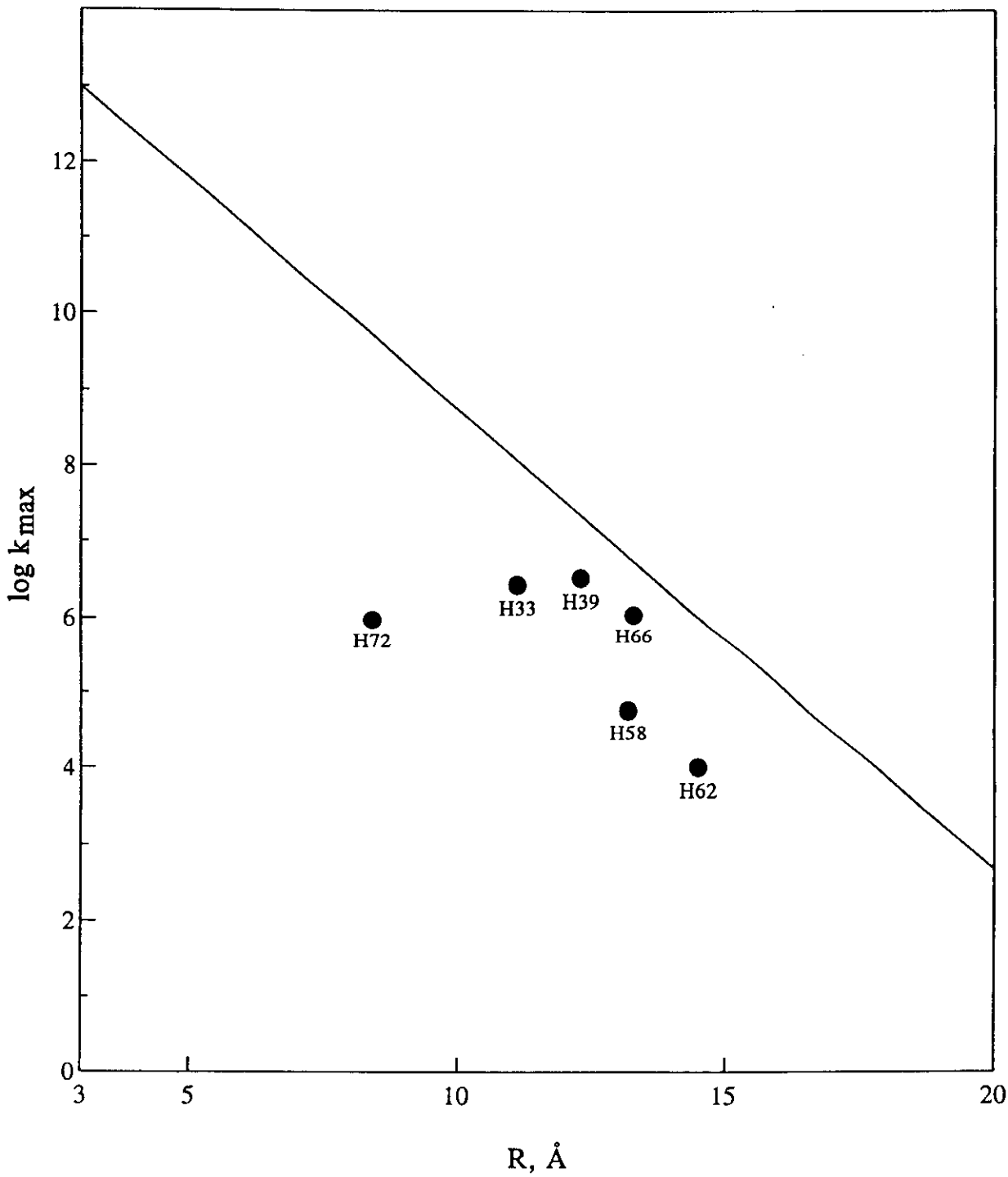

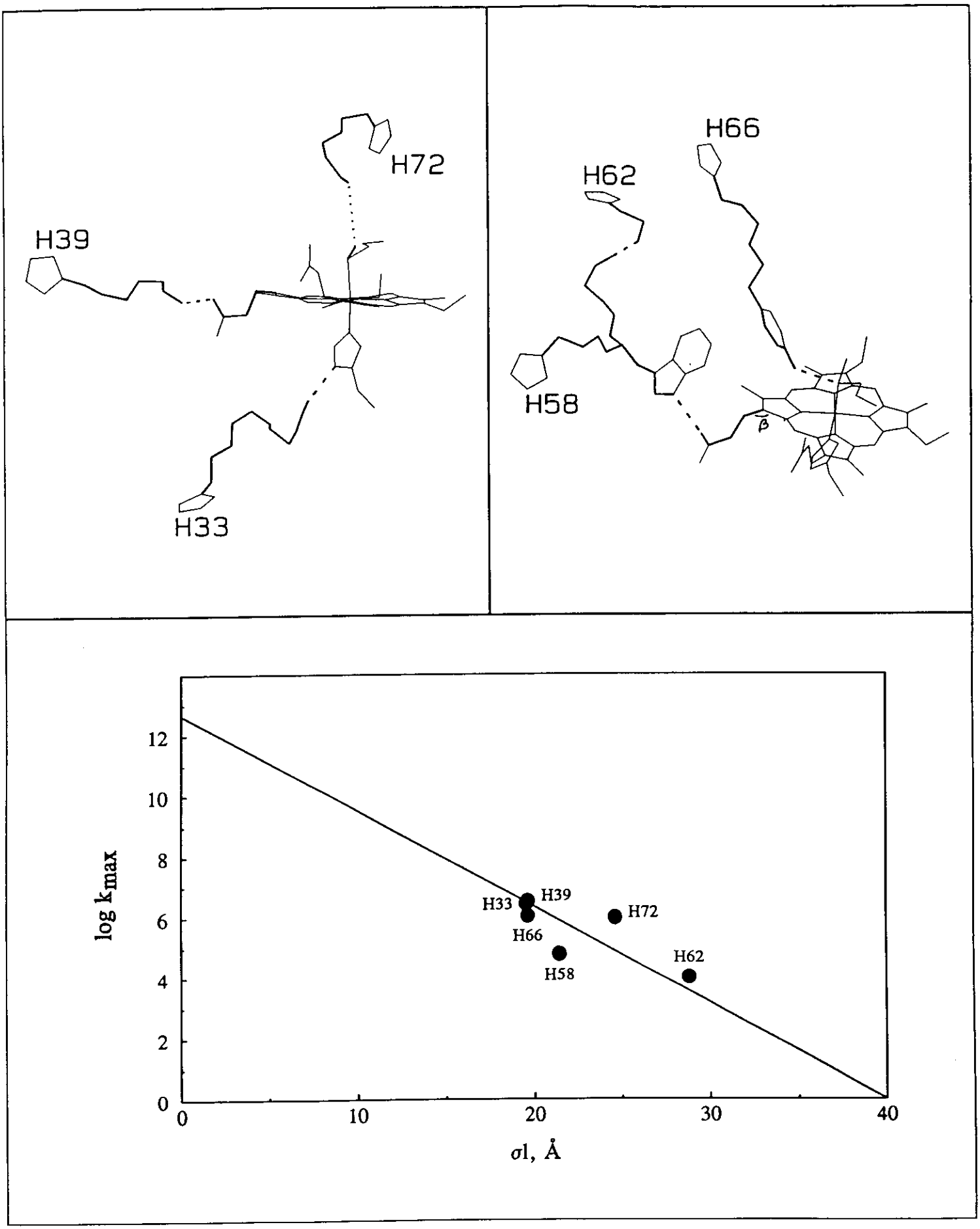
H72
H39
H33
H66
H62
H58
β
log k_{max}
12
10
8
6
4
2
0
0
10
20
30
40
σl, Å
H33
H39
H72
H66
H62
H58

Figure

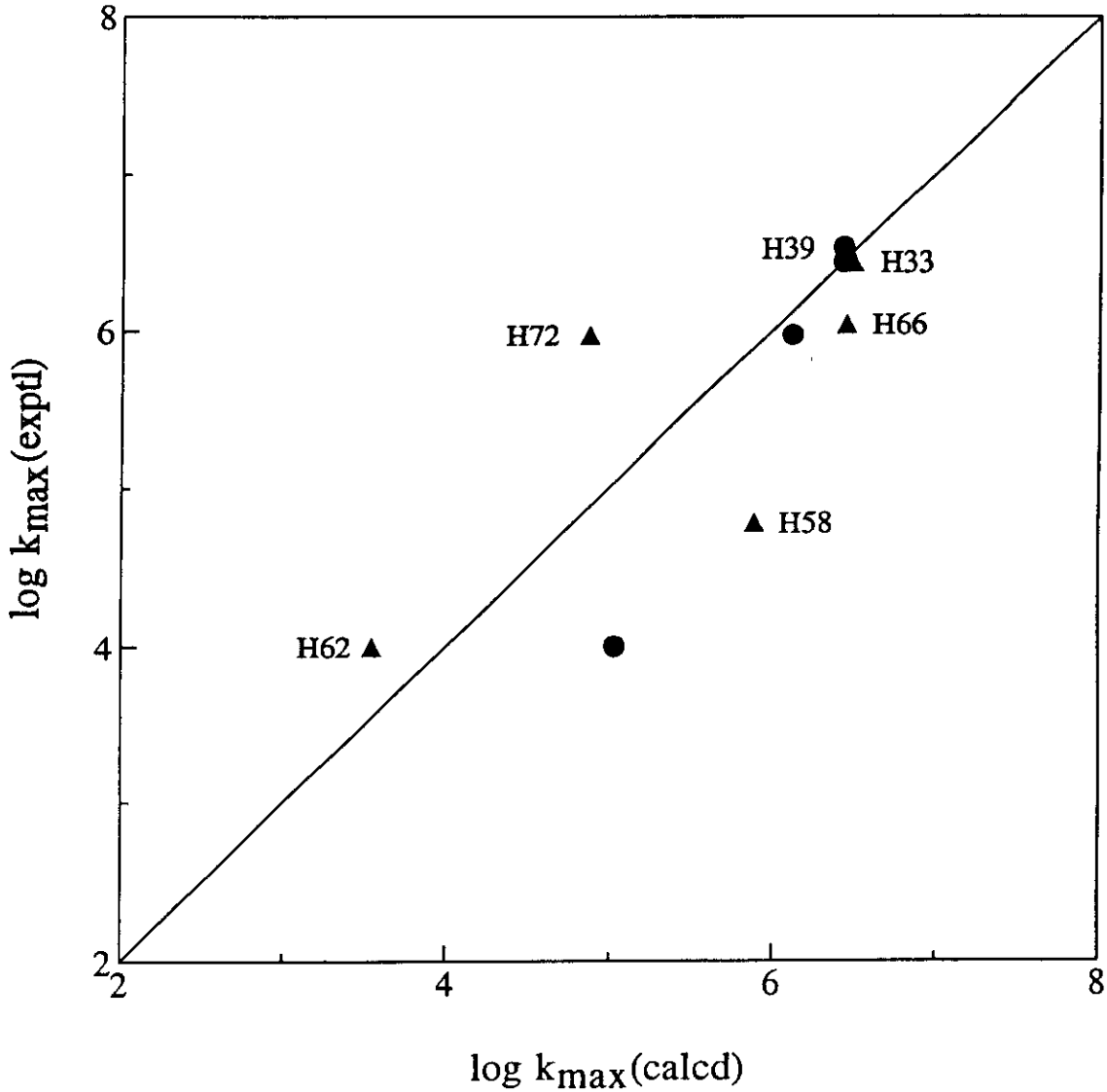
8
6
4
2
2
4
6
8
log k_{max}(exptl)
log k_{max}(calcd)
H39
H33
H72
H66
H58
H62

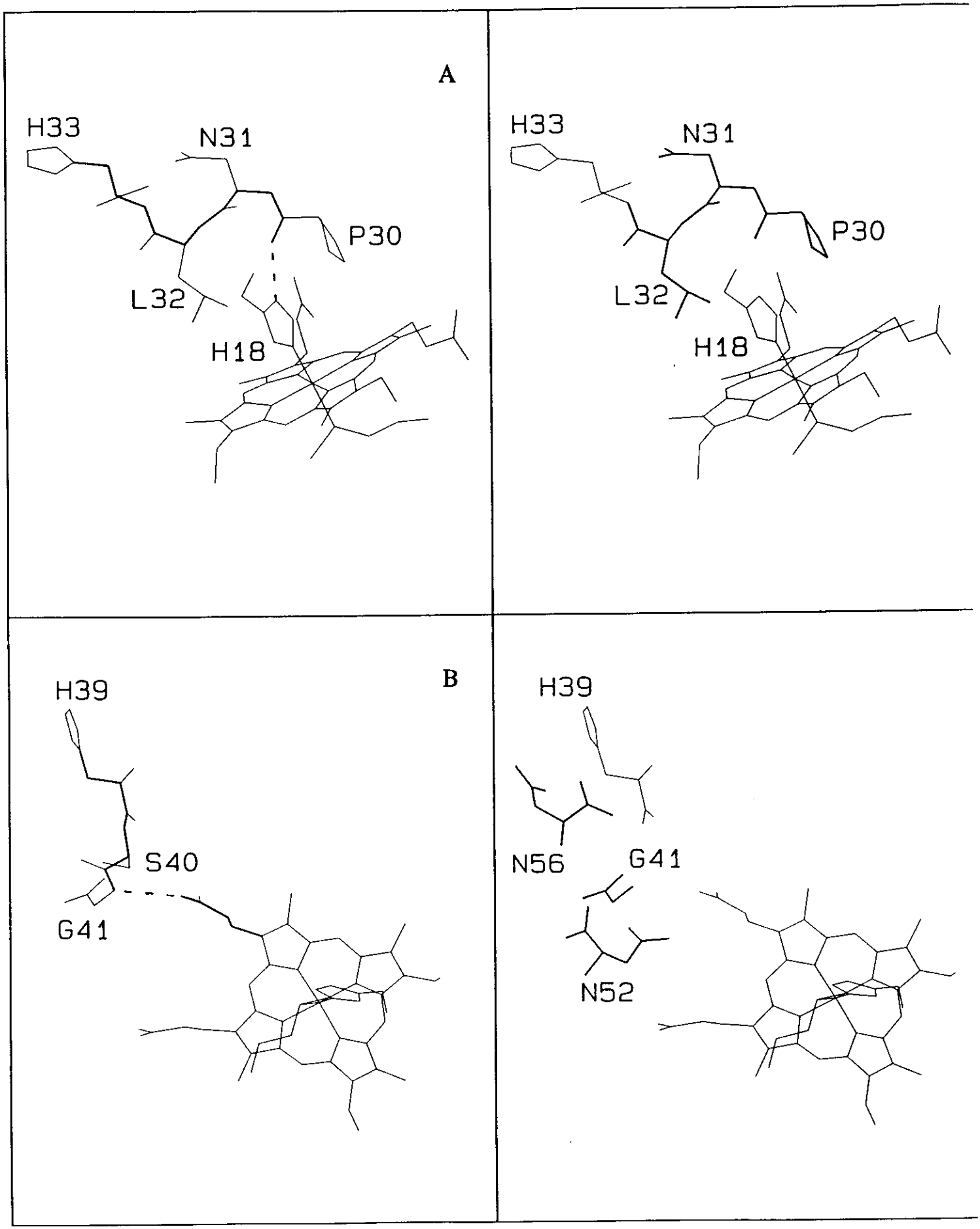
A
H33
N31
P30
L32
H18
H33
N31
P30
L32
H18
B
H39
S40
G41
H39
N56
G41
N52

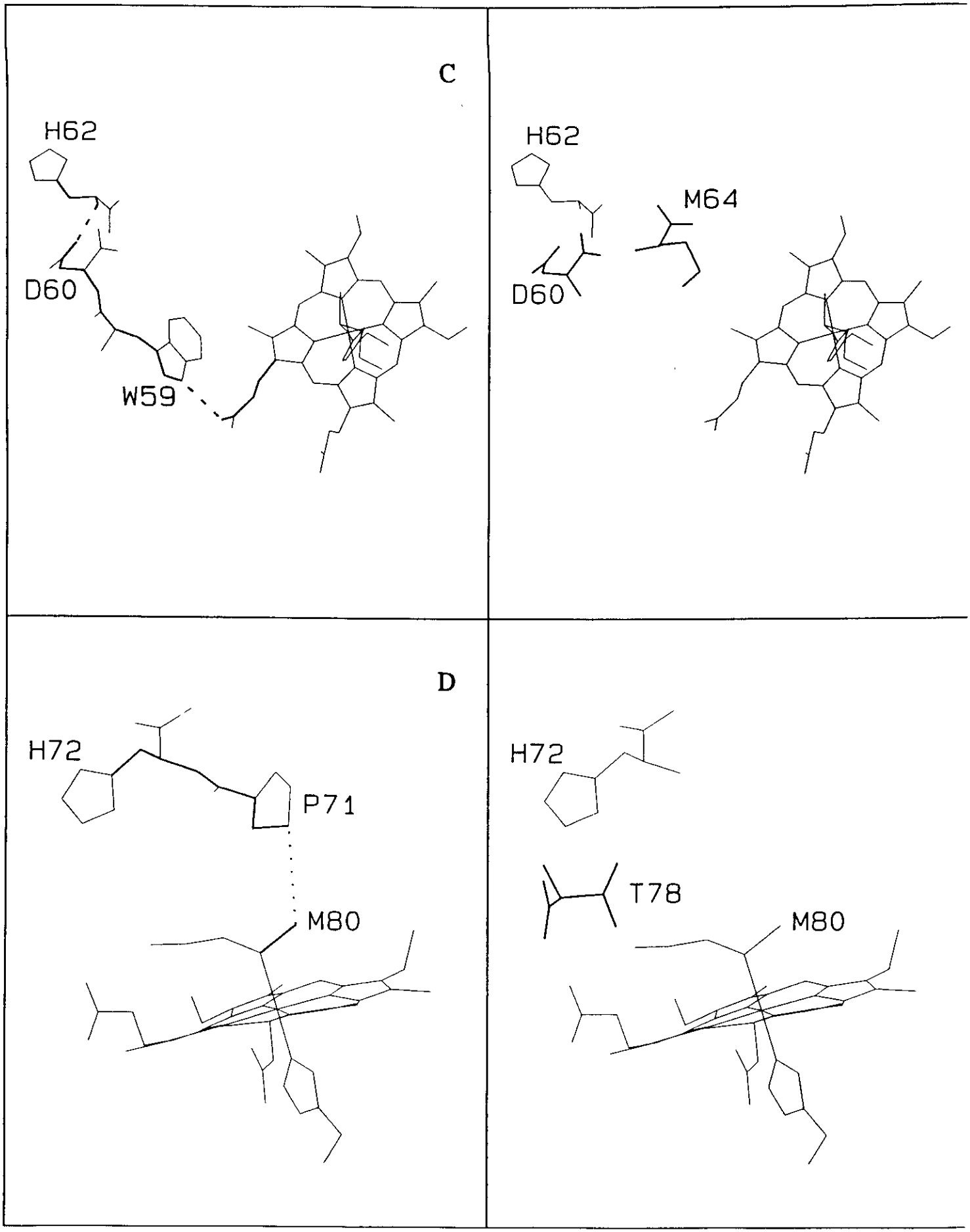
C
H62
D60
W59
H62
M64
D60
D
H72
P71
M80
H72
T78
M80

Figure 5

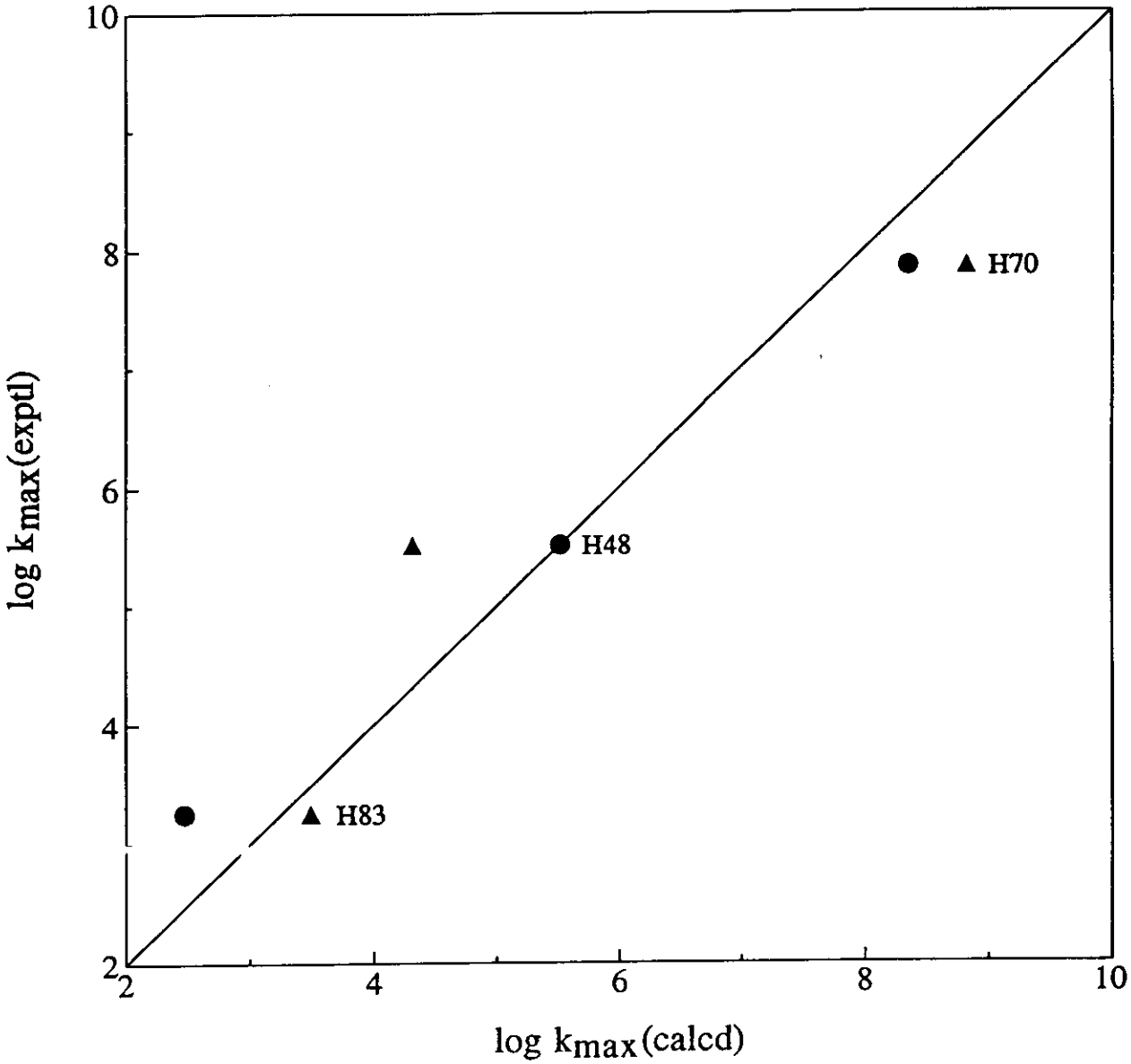

Figure

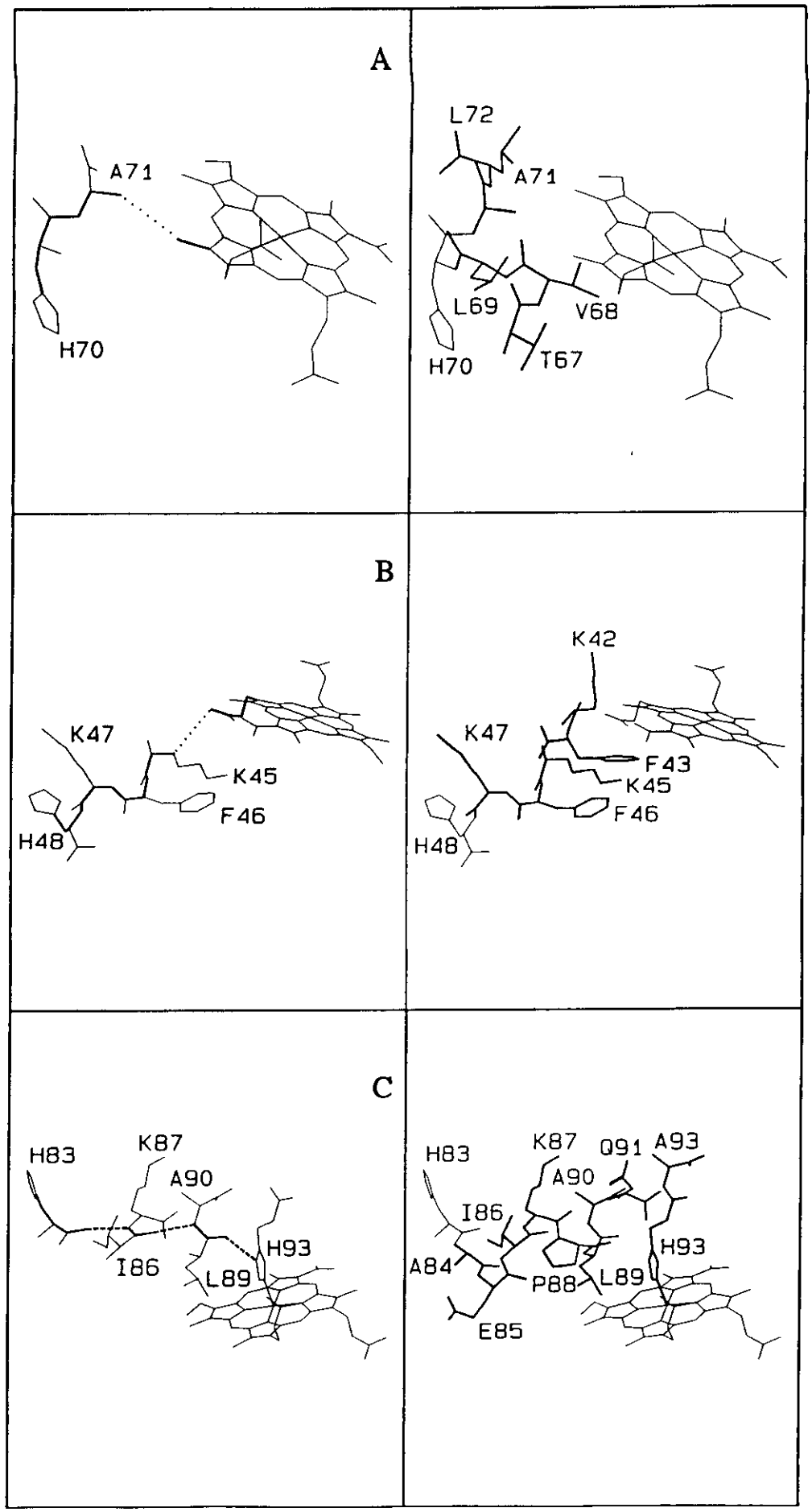
A
A71
H70
L72
A71
L69
V68
H70
T67
B
K47
K45
F46
H48
K42
K47
F43
K45
F46
H48
C
H83
K87
A90
I86
H93
L89
H83
K87
Q91
A93
A90
I86
A84
P88
L89
H93
E85